Summer 8-7-2019

Characterization of Endothelial Nitric Oxide Synthase Serine-600 Phosphorylation

Kevin Patel
Kennesaw State University

Characterization of Endothelial Nitric Oxide Synthase Serine-600 Phosphorylation

by

Kevin K. Patel

Biochemistry

Kennesaw State University, 2019

Submitted in Partial Fulfillment of the Requirements

For the Degree of Master of Science in the

Department of Chemistry and Biochemistry

Kennesaw State University

2019

_____	_____
Committee Chair Coordinator	Graduate Program
_____	_____
Committee Member	Department Chair
_____	_____
Committee Member	College Dean
_____	
Committee Member	

Contents

List of Tables

List of Figures

List of Supplementary Figures

ABSTRACT

Endothelial nitric oxide synthase (eNOS) is part of a family of three nitric oxide synthase (NOS) enzymes that catalyze the production of nitric oxide (NO). NO is a gaseous, free-radical signaling molecule that has a variety of cellular and physiological functions that range from maintaining cardiovascular homeostasis to neurotransmission. The function of NO greatly depends on the concentration and is cell type specific. eNOS is the most regulated of the three NOS isoforms and the mechanisms of regulation can be through protein-protein interactions and posttranslational modifications. A connection with eNOS and the cell cycle has begun to form with recent research identifying eNOS as a substrate of cyclin-dependent kinases (CDK). CDKs are one of the regulatory elements in cell cycle progression and form a class of serine/threonine kinases. The most commonly studied and well understood posttranslational modification of eNOS is phosphorylation. This work builds on our laboratory's discovery of a phosphorylation site – ser^{600} – on the autoinhibitory loop of eNOS. Our work finds a novel connection between phosphorylation at this site and mitosis.

CHAPTER 1 – INTRODUCTION

Nitric Oxide and its Physiological Relevance

Nitric oxide (NO) is a gaseous free-radical molecule that, while short-lived, regulates a plethora of physiological functions that are both concentration and location/context dependent (1-5). For example, in the nervous system, NO can act as a neurotransmitter (4). In the cardiovascular system, NO can act as a vasodilator mediating endothelium-based relaxation of blood vessels (1). Additionally, NO can influence multiple cellular events ranging from apoptosis to cell cycle arrest (2-5). NO has even been implicated in several cancer-related events that include angiogenesis, anti-apoptotic mechanisms, tumor cell invasion, and metastasis (5). Overall, NO is a potent bioactive molecule that influences an abundance of physiological functions.

Physiological dysregulation can arise when too much or too little NO is produced. A high level of NO is associated with oxidant induced pathogenesis which can result in tissue damage and hypertension in the cardiovascular system (6). On the other hand, a low level of NO is associated with compromised immune function, increased development of cardiovascular issues like hypercholesterolemia, and is linked to exacerbation of diabetic symptoms (7).

NO is a free radical and as such, has high reactivity with just about all molecules. Physiologically, NO is not the only free radical that is produced. Some of these radicals can be formed from molecules reacting with NO. In fact, there is reasonable variety in the physiologically relevant intracellular free radicals, shown in table 1 below (8). Each radical

can react with a multitude of molecules ranging from proteins to other signal mediators which can alter normal cellular function.

Table 1: Summary of Different Reactive Oxygen Species and Half-life (8)

Reactive Species	Symbol	Half-life
Superoxide	O_2^-	10^{-6} s
Hydroxyl	HO	10^{-10} s
Alkoxy	RO	10^{-6} s
Peroxyl	ROO	17 s
Hydrogen peroxide	H_2O_2	Stable
Singlet oxygen	$^1O_2$	10^{-6} s
Nitric oxide	NO^-	~ 7 s*
Nitrite	NO_2^-	110 s
Nitrate	NO_3^-	5-8 h
Nitrous acid	HNO_2	-
Peroxynitrite	$ONOO^-$	10^{-3} s
Alkyl peroxynitrite	ROONO	-
Dinitrogen trioxide	N_2O_3	-
Dinitrogen tetroxide	N_2O_4	-

*- Dependent on environment; for example, can last minutes in air saturated solutions

Nitric Oxide Synthases

One of the things that makes NO unique is the short biological half-life it has, which means it must be actively produced when necessary by nitric oxide synthase (NOS) enzymes. Nitric oxide synthases comprise the class of enzymes that is responsible for the production of NO through the conversion of L-arginine to citrulline producing NO (9); this reaction is shown below in figure 1. NOS enzymes have three main isoforms, neuronal (nNOS; NOS1), inducible (iNOS; NOS2), and endothelial nitric oxide synthases (eNOS; NOS3) (10). All three enzymes in the family use the same cofactors including heme, tetrahydrobiopterin (BH_4), flavin mononucleotide (FMN), flavin adenine dinucleotide

(FAD), zinc, and nicotinamide adenine diphosphate (NADPH). All three enzymes form homodimers, which are required for activity (11). All three enzymes carry out the same enzymatic reaction that consumes 2 moles of L-arginine, 3 moles of NADPH, 3 moles of H+, and 4 moles of O_2 to produce 2 moles of L-citrulline, 2 moles of NO, 4 moles of water, and 3 moles of NADP+ (figure 1). While all three enzymes can catalyze the same reaction, the amount of NO produced varies from isoform to isoform with iNOS producing the most, nNOS producing short bursts, and eNOS producing long pulses. The three isoforms also have the same general structure, a bidomain protein consisting of a C terminal reductase domain and an N terminal oxygenase domain with a calmodulin binding site linking the two domains together. Calmodulin binding is necessary to produce NO. One region that is not conserved between all three of the enzymes is a stretch of 52-55 amino acids that forms an autoinhibitory region between the two domains. This region is present in nNOS and eNOS but not iNOS (12). Another difference that exists between the three enzymes is tissue expression. Neuronal NOS is expressed constitutively in peripheral and central neurons (10). Inducible NOS is not constitutively expressed in cells but can be induced to express in nearly all cells as a response to various stimuli, like inflammation (10). Endothelial NOS is constitutively expressed most commonly in endothelial cells but can be found in cells

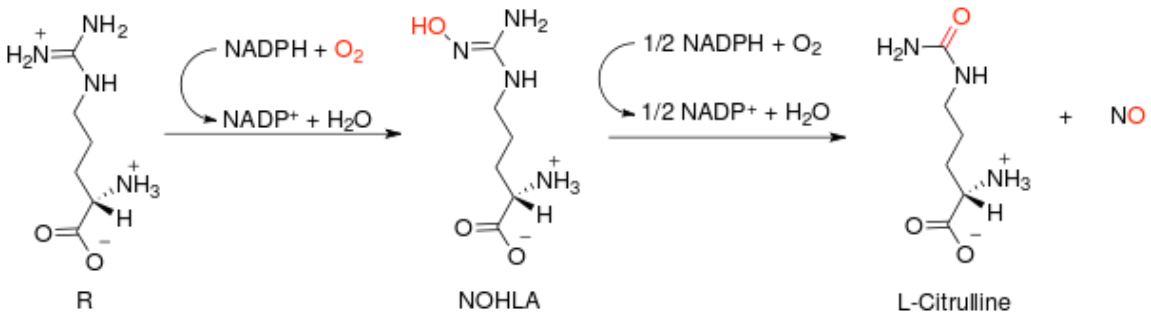

Figure 1: **Nitric Oxide Synthase enzymatic reaction showing conversion from L-arginine to L-citrulline producing NO.** This reaction consumes 2 moles of L-arginine, 3 moles of NADPH, 3 moles of H^+, and 4 moles of O_2 to produce 2 moles of L-citrulline, 2 moles of NO, 4 moles of water, and 3 moles of $NADP^+$.

like the trophoblasts of the human placenta and kidney tubular epithelial cells (10,13). The focus of this study will be on eNOS in endothelial cells.

Endothelial Nitric Oxide Synthase

eNOS is primarily expressed in cardiovascular tissue, specifically endothelial cells (14). The endothelium comprises the inner lining of all blood vessels and is generally divided into two major categories, microvasculature (capillaries) and macrovasculature (arterial and venous). For example, the aorta contains macrovascular endothelial cells whereas dermal capillaries contain microvascular endothelial cells. The endothelium maintains a large amount of eNOS compared to other tissues, this is because NO is potent vasodilator and helps to maintain cardiovascular homeostasis (10). eNOS is also unique among the NOS enzymes due to the degree of posttranslational modifications involved in regulation. Specifically, unlike other NOSs, eNOS is palmitoylated and myristoylated on the n-terminus which allows for localization on the plasma membrane (3). Of these two modifications, palmitoylation is reversible whereas myristoylation is not. In addition to the plasma membrane, eNOS is also found associated with the Golgi apparatus and in the cytoplasm of endothelial cells (15). It has been established that eNOS is found in multiple subcellular pools – plasma membrane, cytoplasm, and the Golgi apparatus (16). However, the full mechanism of how eNOS achieves differential subcellular localization is not clearly understood. The consensus in the literature suggests that eNOS must be on the plasma membrane in order to achieve maximal enzymatic activity. Membrane localization of eNOS allows for diffusion of NO across the membrane onto the underlying smooth muscle tissue which results in the signal for vasodilation. The Golgi pool of eNOS is less active compared to membrane associated eNOS, likely due to limited access to substrates.

Regulation of Endothelial Nitric Oxide Synthase through Phosphorylation

The most commonly studied form of eNOS regulation is through phosphorylation which has resulted in the identification of multiple phosphorylation sites. Each site influences eNOS differently resulting in functional enhancement, inhibition, or a change in cellular interactions. Most of the identified phosphorylation sites on eNOS are serines or threonines. Of them, the first identified and most commonly studied site is ser^{1177}; modification at this residue enhances NO production by enhancing electron flow in the reductase domain which increases the activity of eNOS (17, 18). Additional known activation sites include ser^{615} and ser^{633} (19, 20). The most well studied inhibitory site is at thr^{495}; phosphorylation at this residue blocks calmodulin association and therefore ablates NO output (21). Other phosphorylation sites are present on eNOS but have some ambiguity with regards to altering NO output. One site, ser^{114}, has been shown to be inhibitory *in vivo* not *in vitro*, with the current consensus suggesting that phosphorylation at this residue increases association of eNOS to negative cofactors resulting in reduced *in vivo* activity (22, 23). Our lab has recently identified a new phosphorylation site, ser^{600} (24). Ser^{600} is found in the eNOS autoinhibitory loop near two activating sites, ser^{615} and ser^{633}. Additionally, two tyrosine phosphorylation sites have also been identified on eNOS, tyr^{81} and tyr^{657} (25-27). Phosphorylation at tyr^{81} has been shown to be activating while tyr^{657} is thought to be inhibitory (26). Despite the numerous phosphorylation sites, little investigation has been done on their regulation during the cell cycle which opens another potential avenue understanding for eNOS function and regulation. Known phosphorylation sites are summarized in Table 2.

.

Table 2: Summary of the phosphorylation sites of eNOS and the resulting difference in NO output by residue type

Residue Type:	Residue Number:	Activating/Inhibiting	Reference
Serine	114	Inhibiting (*in vivo)*	22-23
	600	Inhibiting *(in vitro*)	24
	615	Activating	19
	633	Activating	20
	1177	Activating	17-18
Threonine	495	Inhibiting	21
Tyrosine	81	Activating	26
	657	Inhibiting	26

Endothelial Nitric Oxide Synthase and the Cell Cycle

Recently, evidence suggests that eNOS may play a role in cellular proliferation by interacting with a variety of genes (28). One study identified that eNOS deficiency in mice resulted in reduction of collateral vessel density due to impaired activation of a cell cycle gene network during arteriogenesis. Additionally, the same group found that eNOS maintains a role in collateral remodeling by regulating cell proliferation (28). Collateral blood vessels are abnormal blood vessels which connect the aorta to pulmonary arteries. Arteriogenesis is like angiogenesis but refers to increasing the size in the diameter of existing arteries rather than the formation of new vessels entirely. Furthermore, the same study found that, eNOS knockout mice were not able to upregulate between 40-44 genes related to the cell cycle and could result in altered cell cycle progression (28). In other studies, transfer of the NOS 3 gene into vascular smooth muscle and human embryonic kidney cells was shown to inhibit cellular proliferation in both types of cells (12, 29). Ultimately, there is limited data available in the literature that directly measures the impact

of eNOS on cell cycle progression, further research is necessary to establish the nature of the linkage.

There is considerable evidence that suggests eNOS may be actively regulated as the cell cycle progresses as part of global cellular mechanisms of regulation like phosphorylation. Two separate research groups have shown that eNOS is phosphorylated by CDK 1 and CDK 5 at ser^{114} (30-31). Phosphorylation of ser^{114} caused lowered nitrite production in SH-SY5Y cells transfected with both eNOS and CDK5/p35 (30). Additionally, CDKs 1, 2, and 5 were shown to phosphorylate ser^{114} *in vitro* and treatment with roscovitine, a CDK 1, 2, and 5 inhibitor prevented phosphorylation *in vivo* (31) This opens the possibility that eNOS may be regulated through CDKs. Another study has shown that VEGF mediated ser^{1177} phosphorylation is linked to vein formation in embryonic endothelial cells and regulates the formation of blood vessels (32). Besides phosphorylation, eNOS is regulated through interactions with other proteins like calmodulin. Another protein that interacts directly with eNOS is NOS interacting protein (NOSIP). NOSIP has been shown to interact with eNOS in a cell cycle dependent mechanism and is a nuclear ubiquitin ligase that is released to the cytoplasm as part of late cell cycle (33). Specifically, eNOS was shown to be downregulated during G2 phase through NOSIP-mediated subcellular localization of eNOS to the cellular cytoskeleton. Additionally, the activity of eNOS is lower in G2 compared to G1, this is reversed when NOSIP is knocked down by siRNA (33) Taken together this data opens the possibility that eNOS may be actively regulated during the cell cycle, specifically through an ubiquitination event that is cell cycle dependent. In this study, we present data that supports a connection between the cell cycle and eNOS. We have found that eNOS is increasingly

phosphorylated at ser^{600} during mitosis in human microvascular endothelial cells using immunofluorescence, flow cytometry, and western blot analysis.

CHAPTER 2 – EXPERIMENTAL

Structure-based Sequence Alignment

Materials

eNOS sequences were collected from the Swiss UniProt database manually. Sequences were aligned using the MUSCLE algorithm in Jalview 2.10.5. Jalview and Microsoft Word were used to analyze aligned eNOS sequences. A threaded model of the unstructured region of eNOS was made using Swiss-Model. The model was analyzed and refined in PyMol 2.3.2.

Methods

eNOS protein sequences were collected using the "Add to basket" feature on the Swiss UniProt website following a blast query using the protein sequence of human eNOS. Sequences were only selected if more than 70% sequence homology was observed. Sequences were then compared to nNOS and iNOS and excluded if the PDZ domain and autoinhibitory loop matched nNOS or if no autoinhibitory loop was present. This resulted in a collection of 84 eNOS protein sequences from a variety of chordate species, primarily mammalian but also including some reptiles. It is worth noting that if this study is repeated, additional nonmammalian sequences should be collected. The collected sequences were downloaded in FASTA format and imported into Jalview and aligned using the MUSCLE alignment preset. The rendered sequence alignment was then truncated from the full length eNOS to only include the alignment region that matches with amino acid residues 566-674 of human eNOS which includes the autoinhibitory loop. This region was then blasted on the Swiss UniProt website to determine a protein of high homology and resolved structure.

Based on this query, the human iNOS reductase and calmodulin complex flavodoxin-like domain was found (PDB 3HR4 (35)). The human eNOS flavodoxin-like domain from amino acid residue 520 to 703 was then queried into the Swiss-Model using 3HR4 as a template to create a threaded model of the autoinhibitory loop (AIL) of eNOS. The model of the AIL was then opened in PyMol and aligned to the flavodoxin-like domain of iNOS from 3HR4. Regions of structural homology in the model that correspond to the structure from 3HR4 were rendered in color and regions of unknown structure, mainly encompassing the autoinhibitory loop, were left gray. Using the sequence alignment, outliers were removed that maintained low homology in the AIL, and regions of structural homology were color coded to match the model in Microsoft Word.

Cell Culture

Materials

HMEC-1 cells (CRL-3243) were purchased from the American type culture collection (ATCC). MCDB 131 and hydrocortisone were purchased from Sigma-Aldrich. Epidermal growth factor (EGF), L-glutamine, and trypsin were purchased from Genesee scientific. Fetal bovine serum (FBS; E17063) was purchased from Atlanta Biologicals.

Methods

Human microvascular endothelial cells (HMEC-1) were cultured as directed by the ATCC in MCDB 131 media with 10% FBS, 10 ng/mL epidermal growth factor, 1 µg/mL hydrocortisone, and 10 mM glutamine. Fully supplemented media is referred to as complete media. The cells were grown at 37 degrees C in a humidified environment with 5% CO_2 and passaged once 80-90% confluency was reached. Experiments used cells between passages 4-13 and were seeded into vessels dependent upon the experiment being

done – see the subsections for each method to determine what vessel was used and how it was seeded.

For maintenance passages in a T75 flask, media was aspirated, and cells were washed once for 45-60 seconds with 2 mL of trypsin which was then aspirated out of the flask. The cells were then trypsinized off the surface with 3 mL of trypsin incubated for 5 minutes at 37 degrees C. It is worth noting that HMEC cells tightly adhere to surfaces so additional time may be required to remove all the cells from the surface. The trypsin was quenched with 1:1 ratio of complete media to trypsin. Then a portion of the quenched solution of trypsin and cells was moved into a T75 flask, at a dilution appropriate for the density of cells in the flask and the density desired. For example, consider a 1:3 dilution, 2 mL of the cells in a trypsin/media mixture were added to 10 mL of complete media which was then placed into a T75 flask for a total volume of 12 mL. For experiment use, all of the steps are repeated, however instead of moving the quenched solution into a flask, a sample was collected, and the cells were counted before diluting the cells to the desired number and volume prior to placement into the experiment specific vessel.

G2/M cell cycle synchronization

Materials

RO-3306 was purchased as a 10 mM stock in DMSO from MedChemExpress.

Methods

Cells were synchronized at the G2/M barrier using a CDK 1 inhibitor, RO-3306. The inhibitor was added to a final concentration of 5 μM to adherent cells in experiment specific vessels from a 10 mM stock solution prepared in DMSO (Med Chem Express).

The inhibitor treatment lasted 20 hours, then cells were washed once with unsupplemented MCDB 131 then complete media was added to initiate the time course. The amount of media added was dependent on the experimental method being used. The washout of the RO-3306 releases the cells from the G2/M barrier resulting in elevated populations of mitotic cells. It is worth noting that before use of this inhibitor, serum starvation was attempted to synchronize cells, however, the HMECs are hardier than anticipated and a 20 hour serum starvation was not enough to arrest cells in G0. Therefore, if serum starvation is used in the future, a minimum of 24 hours, preferably 48 hours should be utilized.

Immunofluorescence

Materials

Lab-Tek 16-well Chamber Slide and coverslips (178599 and 171080) were purchased from ThermoScientific. PBS supplemented with calcium and magnesium (25-508CB) was purchased from Genesee Scientific. 20% PFA (15713) was purchased from Electron Microscopy Sciences. Horse serum was purchased from Atlanta Biologicals. See appendix for primary and secondary antibodies and dilutions of antibodies used.

Methods

HMEC-1 cells were collected as previously described and seeded into 16-well chamber slides at a density of 0.5 x 10^4 in 100 µL of media. After experimental treatment, cells were fixed with 4% PFA in PBS for 15 minutes at room temperature. Cells were then washed with 100 µL of PBS per well three times, then simultaneously blocked and permeabilized with 5% horse serum and 0.3% Triton x-100 respectively in PBS. All primary antibody staining was done overnight at 4°C with antibody specific dilutions – listed in the appendix – prepared in blocking buffer (5% horse serum, 0.3% Triton X-100,

and 0.01% sodium azide in PBS). After primary staining, cells were washed three times with 100 μL of blocking buffer per well. Then secondary antibody staining was done at room temperature for 45 minutes with manufacture recommended dilutions – also listed in the appendix – prepared in blocking buffer. Cells were washed two times with blocking buffer. Then nuclei were stained with DAPI in PBS, then cells were rinsed with PBS. The wells on the chamber slide system were then removed with brute force and the underlying silicon gasket was carefully lifted using fine tipped forceps. Once the gasket was removed, the slide was rinsed in PBS once, then mounted with Vectashield H-1000. Slides were imaged on a Zeiss LSM 700 confocal microscope. Images were processed and analyzed using Zeiss Zen Black and Blue software.

Flow Cytometry

Materials

Sterile 5-mL polypropylene tubes (21-125) were purchased from Genesee Scientific. RNase A (120-91-021) was purchased from Invitrogen. Bovine serum albumin (BSA) was purchased from Fisher Scientific.

Methods

HMEC-1 cells were seeded into experiment specific containers with experiment specific seeding densities. Depending on the experiment, the cells were or were not treated with RO-3306. Following the treatment or lack of treatment, cells were trypsinized following the same protocol as for passaging cells with the alteration of including 3% BSA in PBS for quenching the trypsin instead of complete media. The cells were then spun down at 200xG for 5 minutes, then the quenching solution was aspirated and 1% PFA in PBS was added to fix the cells in suspension. The cells were fixed for 15 minutes at room

temperature, then the cells were washed with 2 mL of PBS, spun down at 200xG for 5 minutes, and then supernatant was collected into PFA waste. The cells were then blocked, permeabilized, and RNase treated for 30 minutes with 3% BSA, 0.1% Triton X-100, and 100 μg/mL of RNase A in PBS. The cells were then filtered through a 30 μm mesh and counted, cells were then resuspended to 10E6 cells/mL in 3% BSA in PBS. Then, 300 μL of cells were aliquoted into 5-mL sterile cell culture tubes – ensuring that an unstained and single stain samples were also collected – see the table below for an example of how cells were divided for an experiment. The ser^{600} phosphospecific antibody primary was diluted in 3% BSA in PBS and added to the cells to a final dilution of 1:200 for primary staining. The eNOS-Alexa Fluor 647 conjugated primary was used as the manufacturer specified, 20 μL / 100,000 cells. The primary was incubated for 30 minutes at room temperature. The cells were then washed by centrifugation with 4 mL of ice cold 0.5% BSA in PBS at 200xG for 5 minutes. The secondary staining was also done following manufacturer recommended dilutions with the same conditions as the primary staining. Propidium iodide was added to 50 μg/mL final concentration to the secondary staining solution to simultaneously stain DNA and detect the primary antibody with a labeled secondary antibody. Finally, excess antibody and PI was washed out by centrifugation with the same conditions as for washing out the primary. The cells were resuspended in approximately 250 μL of PBS and samples were then run through a BD Accuri C6 flow cytometer with a fast flow rate with an unlimited volume until almost the entire sample was read. Data was analyzed using FlowJo 10.

Western Blotting

Materials

Gel electrophoresis and western transfer reagents were made in house. Mini protean TGX 8-16% gradient gels (Ref #: 456-1103), gel electrophoresis equipment, and western transfer equipment were purchased from Bio-Rad. Prometheus OneBlock Western-FL Blocking Buffer was purchased from Gennesee Scientific. TBST was made in house. Protease inhibitor cocktail and Pierce 660 nm protein assay reagent were purchased from ThermoScientific. See appendix for primary antibodies and dilutions of antibodies used.

Methods

Approximately 7 x 10^5 HMEC-1 cells were seeded into 8 10 cm^2 dishes and allowed to grow for 1.5 days before treatment with RO-3306 or DMSO for 20 hours. After treatment, the RO-3306 inhibitor was washed out of the 8 dishes of cells, each with slightly differing conditions – vehicle (DMSO), 0 mins, 15 mins, 30 mins, 45 mins, 60 mins, 90 mins, and 120 mins after washout. This allows for a time course with time points that captures cells as they initiate and progress through mitosis. Cells were harvested by lifting with a cell lifter into ice cold lysis buffer (150 mM NaCl, 50 mM Tris-HCl (pH 7.4 at 4C), 1.5 mM $MgCl_2$, 10% glycerol, 1% Igepal, and 0.5% Triton X-100) supplemented with 1X protease inhibitor cocktail, 1 μM micro-cysteine, and 2 μM sodium vanadate. Lysates were flash frozen with a splash of liquid nitrogen and placed into the -80C for storage until sample preparation. For sample preparation, lysates were spun down at 18,000xG, the supernatant was collected, and the pellet was discarded. A Pierce 660 nm protein assay was done using samples of the supernatants as specified by the manufacture for a microplate assay. Once the protein concentration was determined, samples were prepared by adding

4X sample buffer with 100 mM DTT to a final concentration of 1X and 25 mM DTT. Samples were then boiled for 5 minutes while a calculation was performed to determine the volume of each sample necessary to load 15 μg of protein onto a 10% SDS gel. Gels were run at 30 mA until the dye front had run off the gel. Proteins were then transferred onto PVDF membrane using the tank method for western transfers. The condition for transfers was 100 V constant for 60 minutes at 4C. Blots were blocked for 1 hour in OneBlock. Primary antibodies were diluted in OneBlock to manufacturer recommended specifications – see appendix for specific dilutions used – and incubated overnight at 4C. Blots were washed 5 times total – 1 fill and dump, 3 5-minute washes, and 1 fill and dump in that order – with TBST. Secondary was diluted in OneBlock to a final dilution of 1:15000 and blots were incubated for 45 minutes at room temperature. The blot was washed the same as after primary antibody staining and scanned on a Licor Odyssey and data was analyzed using ImageStudio 5.2.

CHAPTER 3 – RESULTS

The autoinhibitory loop is highly conserved

Comparison of primary eNOS sequences from 50 different species shows that the autoinhibitory loop (AIL) is highly conserved across the species studied (figure 3). The sequence alignment is highlighted based on homology to *Homo sapien* eNOS. The mammalian sequences are conserved throughout the entire AIL (shown in grey in figure 2) with the most significant variation existing at the val^{616}, which is conservatively substituted for an isoleucine in some mammals including humans. This conservative mutation likely stems from a base substitution event at the first base in the codons ATT, ATC, or ATA for valine to GTX for isoleucine where X is any base. When comparing eNOS orthologs from closely related taxonomic orders, we observe some minor divergences. Specifically, serine residues substituted for threonine residues and lysine residues for arginine residues occur, but these alterations are unlikely to change the overall structure or activity of the protein. Only one organism is shown per genus, also some exceptions were encountered like *Ursus americanus* where insertion or deletion events have significantly altered the AIL, but these were removed from the final sequence alignment.

Phosphorylation sites on eNOS are conserved

Many of the phosphorylation sites that influence activity changes in eNOS are highly conserved throughout mammalian eNOS orthologs. These sites include tyr^{81}, thr^{495}, ser^{615}, ser^{633}, tyr^{657}, and ser^{1177}, where the substrate specificity is maintained upstream and downstream of the phosphorylation site. Ser^{114} is conserved in mammals but some variation occurs in the substrate specificity sequence. In primates, the amino acid after ser^{114} is

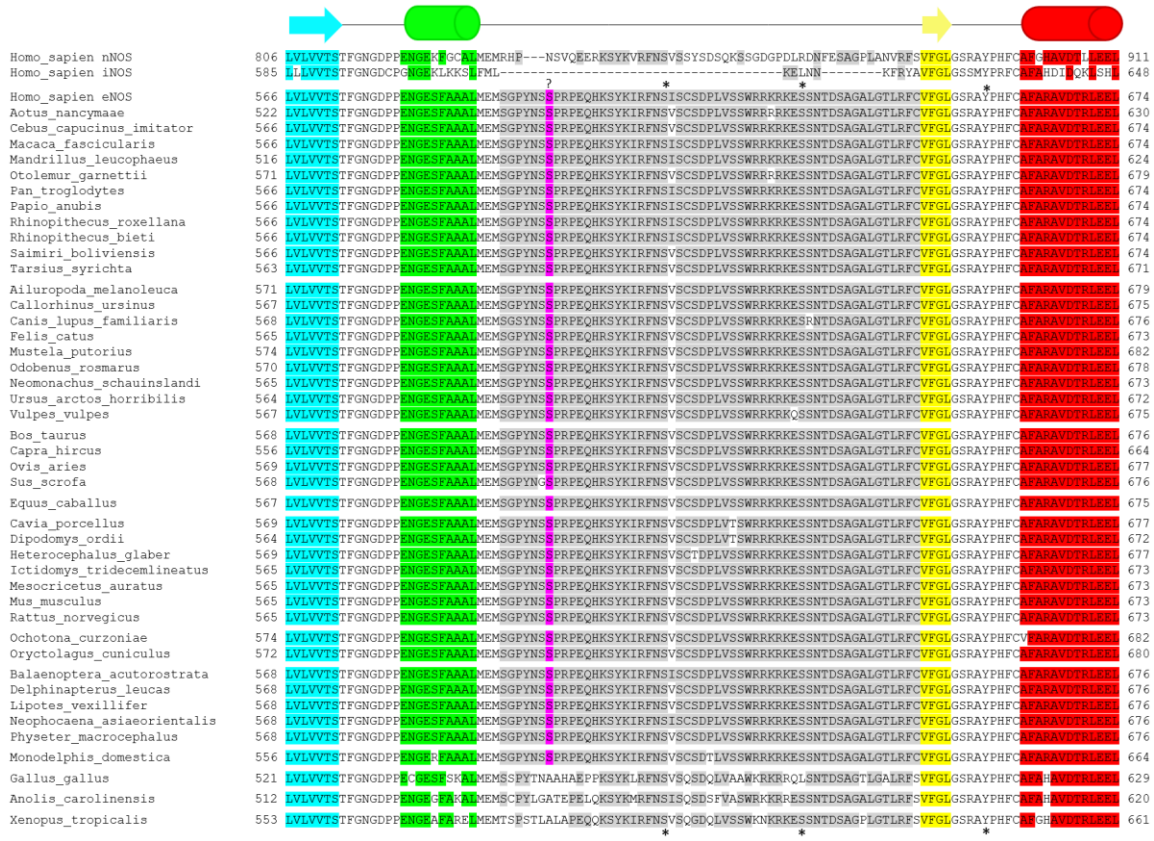

Figure 2. **Alignment of human nNOS, human iNOS, and chordate eNOS sequences highlighting structural similarities**. Colored residues represent conserved structural elements and are highlighted when identical to human eNOS. Highlighted colors correspond to secondary structural elements found in the structural model of the eNOS flavodoxin-like domain shown in figure 4. Arrows indicate beta strands and cylinders indicate alpha helixes. Conserved phosphorylation sites are indicated by an asterisk. Ser^{600} is highlighted in purple and indicated with a "?" on the sequence. The autoinhibitory loop is highlighted in grey.

pro^{115}, but this proline is replaced with a glutamine in other closely related mammalian orders which would likely change the kinase capable of phosphorylating this site to a kinase that is not proline directed. Ser^{615}, ser^{633}, and tyr^{657} are indicated by an asterisk on figure 2. Phosphorylation sites significantly distant (tyr^{81}, ser^{114}, thr^{495}, and ser^{1177}) from the AIL are not shown in figure 2. Ser^{600} is highly conserved in mammals and marsupials, but not conserved in eNOS orthologs from more divergent taxonomic orders like birds, amphibians, and reptiles (shown without ser^{600} in the lower portion of figure 2). This suggests that ser^{600} may have some evolutionary significance in mammalian eNOS

orthologs. This observation is supported by the phylogenetic tree of NOS enzymes published by Andreakis et al (34). Specifically, at the branch point between avian eNOS orthologs and the most common ancestral eNOS ortholog between mammals and marsupials. However, as this information comes from a limited dataset, the study should ultimately be independently repeated with additional data.

Structural elements of the autoinhibitory loop are conserved.

Structurally, the AIL has not been elucidated, likely due to flexibility in that region. In all the crystal structures available for NOS enzymes, this region did not provide electron density and may be a flexible region of the protein with inconsistent positioning in the crystals. The region is highly conserved across mammalia and reptilia. Due to the lack of structural data of the AIL, a threaded model of that loop and the surrounding domain was made using the crystal structure of the flavodoxin-like domain of iNOS found in PDB 3HR4 shown in figure 3. From this model and a comparison of the sequences (figure 2), multiple beta sheets and alpha helixes were found to be conserved (highlighted in cyan, green, yellow, and red in figure 1 to match the colored regions of the model in figure 3). The AIL had virtually no structurally resolved information, the closest comes from rat nNOS reductase domain (PDB 1TLL (36)), but only a few amino acids within the rat nNOS AIL had structural information associated with them resulting in a small resolved helix. However, this helix may not be present in eNOS due to differences in the primary structure around that region. Comparing the primary structure within the AIL between nNOS and eNOS, it appears that eNOS has more hydrophobic residues (leu^{622}, val^{623}, and trp^{626}) which could be contributing to a small hydrophobic pocket that is absent in the nNOS. The

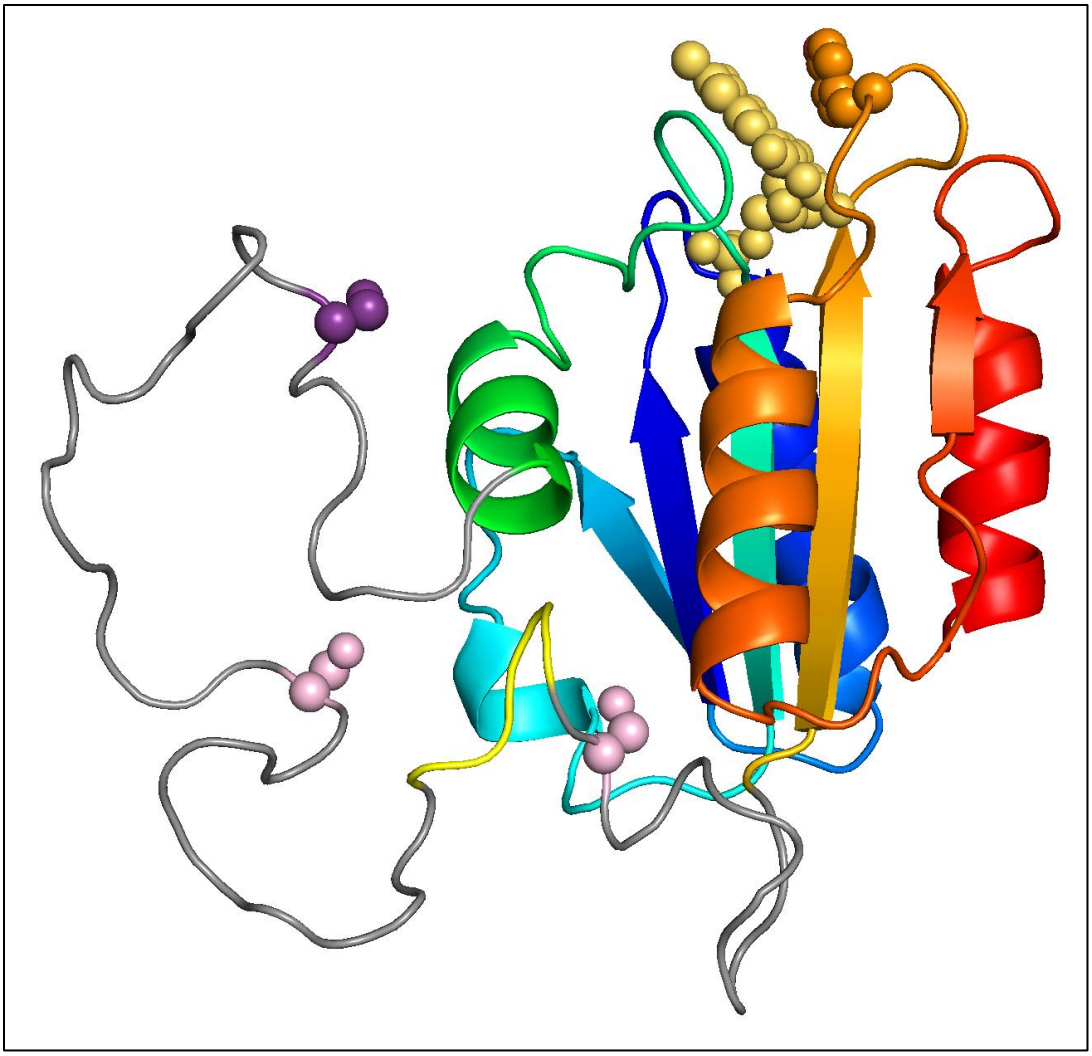

Figure 3. **Structural model of the flavodoxin-like domain of eNOS**. The model was created using Swiss-model with the structure of human iNOS bound to calmodulin used as the template (PDB 3HR4). The colored regions represent areas of high structural homology, whereas the grey region is of unknown structure and encapsulates the autoinhibitory loop of eNOS. Ser^{600} is shown in purple. Ser^{615} and ser^{633} are shown in pink. The proposed MAPK binding domain is shown in yellow in the AIL. Tyr^{657} is shown in orange. FMN is shown in pale yellow.

amino acid residues at these positions in nNOS are small, polar amino acids (ser^{822}, gln^{823}, and ser^{825}). One explanation is that eNOS maintains a small hydrophobic pocket which is absent in at least the reported structure of 1TLL of nNOS. Another explanation could be differences in binding partners for nNOS and eNOS, where the eNOS AIL uses hydrophobic interactions with its binding partners and whereas the nNOS AIL uses charged

interactions with its binding partners. Overall, conclusions are difficult to make about the structural nature of the AIL due to the lack of structural data in that region. However, the distance of ser^{600} from the FMN in the structure, makes it is unlikely that phosphorylation perturbs the electron transport occurring near the FMN and therefore as our most current data suggests (supplemental figure 1), ser^{600} phosphorylation may not influence nitric oxide production directly. However, phosphorylation here could influence eNOS binding partners due to the hydrophobic amino acid residues located near ser^{600} in the model. With regards to the eNOS dimer, ser^{600} is positioned within the FMN binding region of the eNOS monomer. This is not associated with the dimerization interface in either the oxygenase or reductase domain of the eNOS monomer (37).

Ser^{600} phosphorylation is modulated in a small subpopulation of late cell cycle HMEC cells

The physiological significance of phosphorylation of eNOS at ser^{600} has not been characterized. Only one reference exists on this site from our lab. To better understand the importance of this highly conserved site in mammals, we used immunofluorescence to observe P-ser^{600} with a phosphospecific antibody in cycling endothelial cells (figure 4). We found that only a small subpopulation of cells showed significant staining with this antibody. A pattern of the staining was that only cells partially released from the growth surface and cells that were rounded up showed increased staining (figure 4A). This led us to believe that either apoptotic or mitotic cells were showing P-ser^{600}. Based on the DNA morphology, it initially appeared that cells that have heightened phosphorylation at ser^{600} have condensed DNA and are mitotic as two cells are in metaphase and one cell is in anaphase (figure 4A). To follow up on this, flow cytometry was deployed to assess DNA density and to characterize the cell cycle of P-ser^{600} elevated cells (figure 4B). We observed

that P-ser^{600} was found in cells that primarily have N=4 DNA. This indicated that cells positive for ser^{600} phosphorylation were at G2/M phase. Comparatively, cells that show basal staining for P-ser^{600} have cells at N=2, 2<N<4, and N=4 DNA indicating that G1, S, and G2/M phase cells are observed (figure 4B). Additionally, no DNA fragmentation was observed in P-ser^{600} elevated or basal cells leading us to surmise that apoptotic mechanisms are not correlated with the phosphorylation of ser^{600}. Taken together with the DNA staining in immunofluorescence, we believe that ser^{600} phosphorylation is modulated during mitosis in microvasculature, making our lab the first to link this phosphorylation site to other regulatory processes in the endothelium.

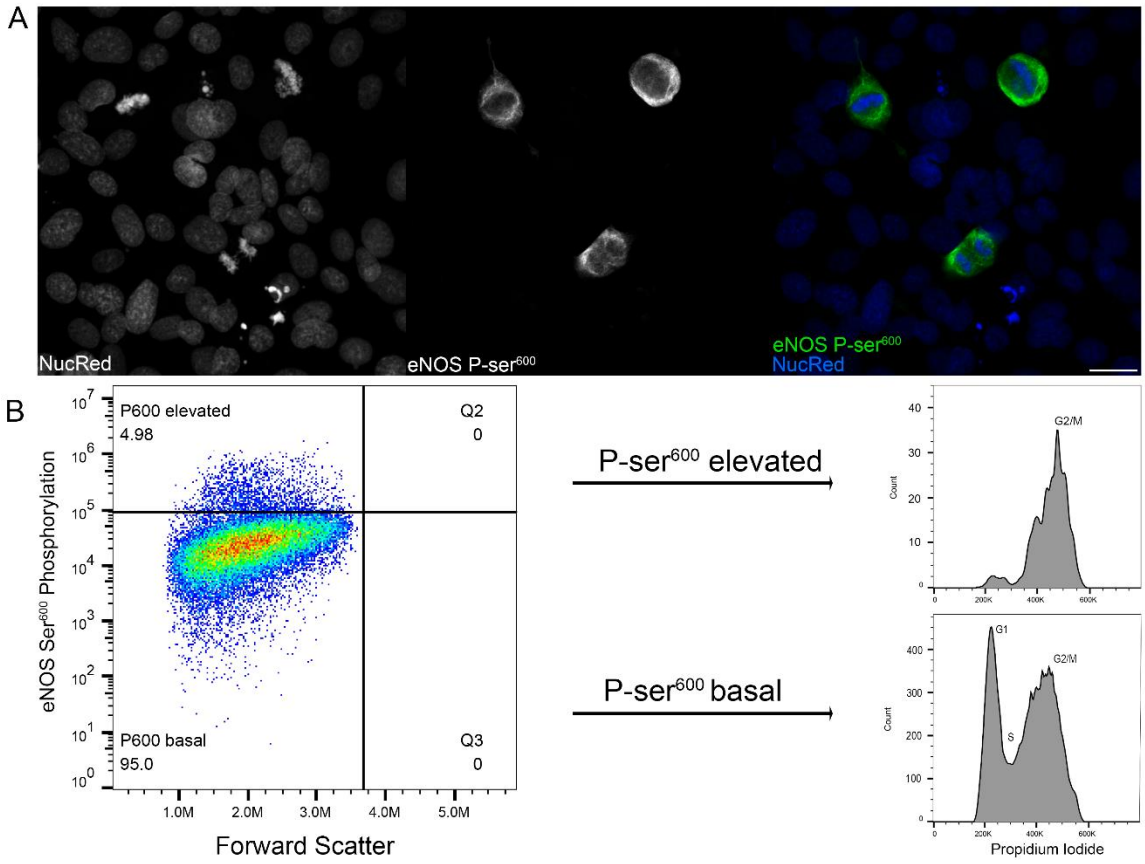

Figure 4. **eNOS ser^{600} phosphorylation is only observed in a subpopulation of cells.** Representative image of indirect immunofluorescence (A) and indirect flow cytometry (B) demonstrating that ser^{600} phosphorylation is observed at high levels a small subpopulation of cells. Observations are representative of four independent experiments. Scale bar represents 20 μm.

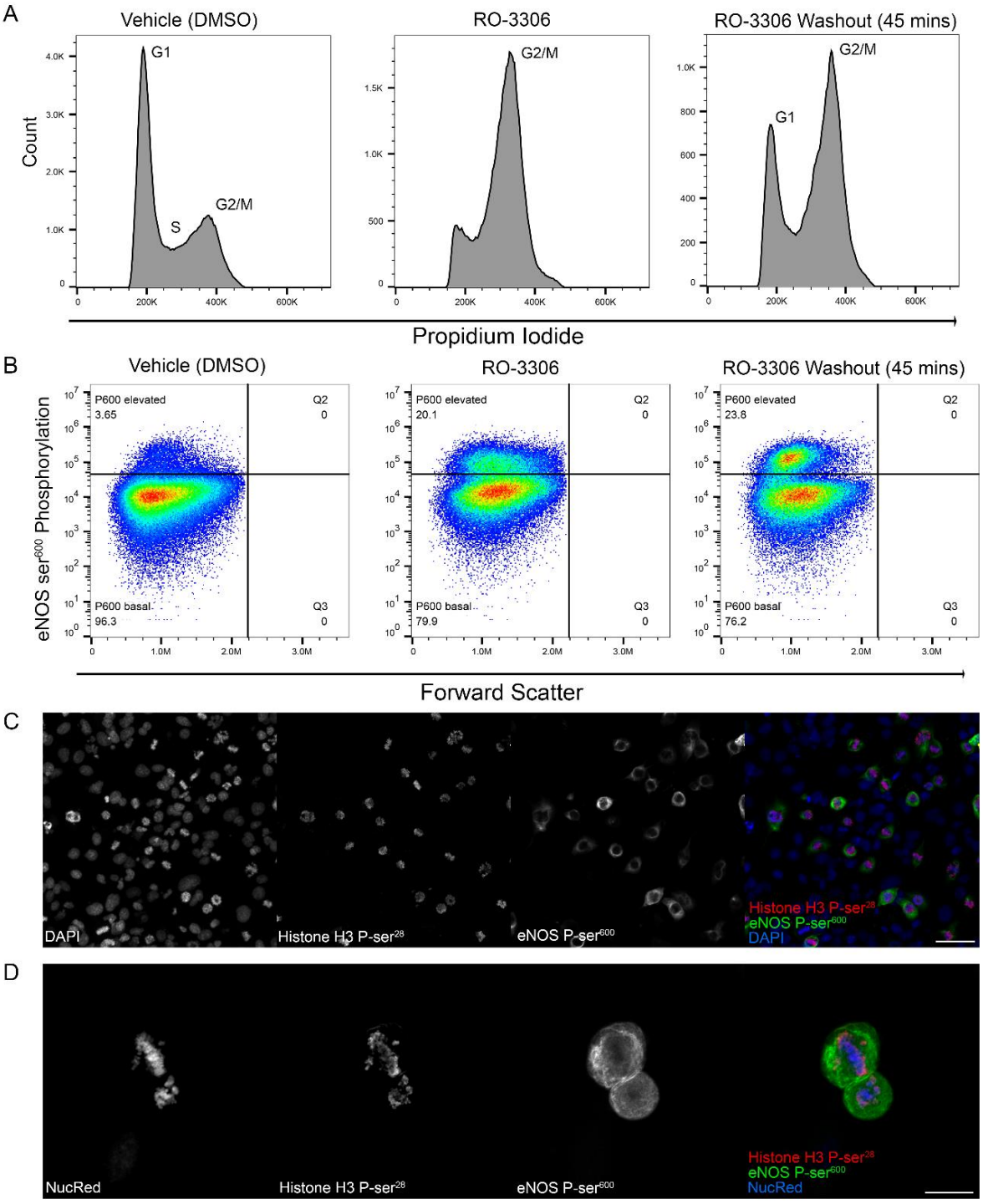

Figure 5. **eNOS ser^{600} phosphorylation is elevated with mitosis.** Representative data of indirect flow cytometry demonstrating that treatment with 5 μM RO-3306 results in reversible G2/M synchronization (A) and that Ser^{600} is elevated by treatment with RO-3306 and washout of inhibitor (B). Representative image of indirect immunofluorescence showing that with washout of 5 μM RO-3306, a G2/M inhibitor, the population of mitotic cells increases as well as ser^{600} phosphorylation, scale bar represents 50 μm (C); a magnified image of two cells in metaphase is shown, scale bar represents 20 μm (D). Observations are representative of three independent experiments.

Ser^{600} phosphorylation is elevated in mitotic endothelial cells

Given that ser^{600} phosphorylation was observed in cells that appear to be in late cell cycle or in G2/M phase based on the DNA content, we further investigated the point of modulation for P-ser^{600} in the cell cycle. To investigate this, we deployed a reversible CDK 1 inhibitor that arrests at the G2/M barrier – RO-3306. Upon washout of the inhibitor, cells rapidly begin mitosis (figure 5A). We observed an increase in P-ser^{600} after RO-3306 treatment (figure 5B). Using immunofluorescence and staining with anti-histone H3 ser^{28} phosphorylation – a mitotic indicator – we observed strong concomitant staining between the two antibodies (figure 5C). Magnification of the staining is shown in figure 5D. This is reflective of P-ser^{600} being modulated during the cell cycle and confirms that P-ser^{600} is modulated in specific circumstances during the start of mitosis and not during G2 phase. Additionally, flow cytometry following 45 minutes after the RO-3306 washout showed roughly 6 times greater proportion of cells P-ser^{600} elevated compared to the vehicle control. Suggesting P-ser^{600} is modulated by a kinase that is activated during early mitosis.

eNOS levels do not significantly change throughout the cell cycle

To ensure that the elevation in P-ser^{600} is not from changing levels of eNOS protein, we employed additional immunofluorescence and flow cytometry. Using an anti-eNOS monoclonal antibody in immunofluorescence, we found that eNOS staining is consistently observed in cycling cells (figure 6A). To analyze a larger number of cells and to assess the cell cycle, flow cytometry was used to observe eNOS while co-staining with propidium iodide to measure DNA content. This showed us that eNOS positive cells were found at all points of the cell cycle (figure 6B). When comparing DNA content to eNOS staining, little difference is observed throughout the cell cycle, with eNOS levels staying at a relatively

consistent level (figure 6C). Taken together, we believe that eNOS levels are remaining consistent throughout the cell cycle and the P-ser^{600} is not elevated due to an increase in eNOS protein.

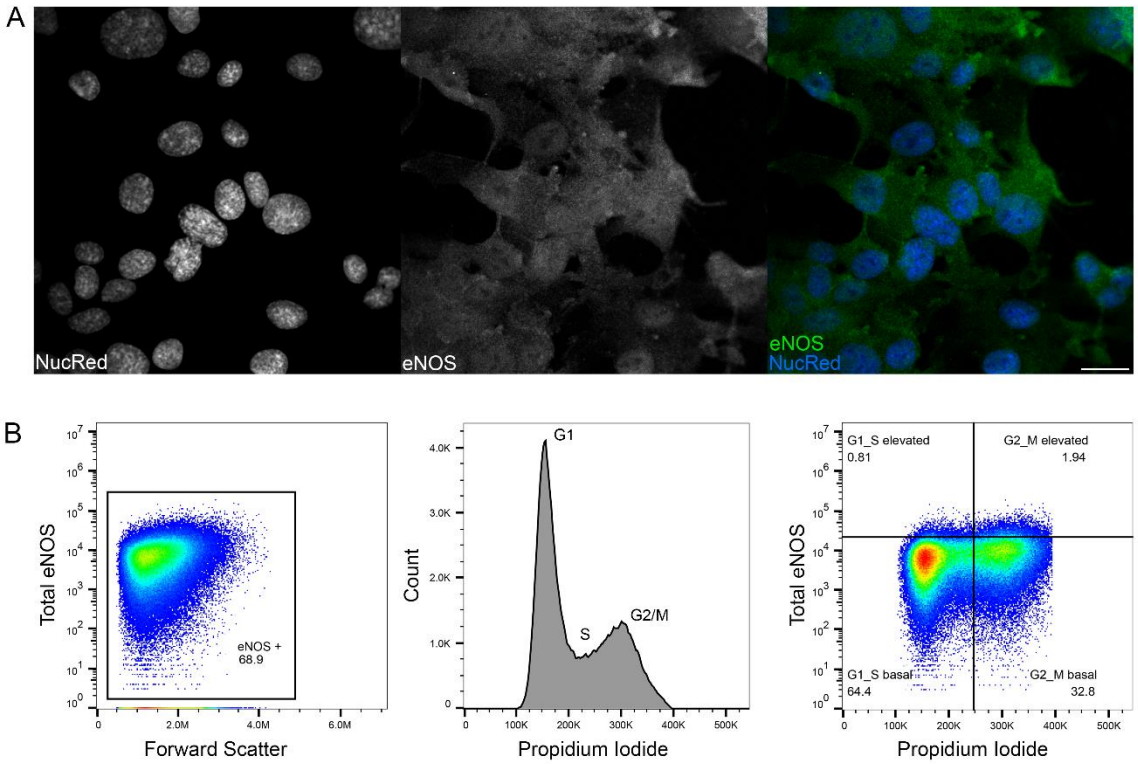

Figure 6. **Total eNOS is observed throughout the entire cell cycle.** Representative image of indirect immunofluorescence (A) and direct flow cytometry (B) demonstrating that eNOS is observed throughout the cell cycle. eNOS protein levels are also relatively consistent throughout the cell cycle when compared to PI staining (C). Observations are representative of three independent experiments. Scale bar represents 20 μm.

Proximity ligation assay verifies P-ser^{600} antibody specificity

To build on our previous publication (24) and further validate our P-ser^{600} antibody specificity to eNOS, we used an *in-situ* proximity ligation assay (PLA) kit from Millipore. This kit was adapted from a publication by Söderberg et al. (38). Simplified, this assay uses the principles immunofluorescence and rolling circle PCR. The immunofluorescence component of the assay used the same steps as normal immunofluorescence, but replaced fluorophore conjugated secondary antibodies with pseudo-secondary antibodies conjugated to DNA oligonucleotides to detect bound primary antibodies – in this case, the

BD Biosciences eNOS monoclonal antibody and our P-ser^{600} antibody. The rolling circle PCR component used three things, additional DNA oligonucleotides to form a complete circular sequence of DNA, a ligase to ligate this circular DNA, and a polymerase to amplify the linear DNA conjugated to the antibody. Detection was accomplished using complimentary DNA oligonucleotides conjugated to fluorophores. Signals using this PLA kit are only produced when primary antibodies are within 40 nm of each other. In our study, we observed little to no signal when no primary antibodies were used (figure 7A). However, when using PLA with an eNOS monoclonal antibody and our polyclonal P-ser^{600} antibody, we observed punctate signals in the periphery of the cell (figure 7B). The punctate signals are in similar position in the cell as observed when staining with the P-

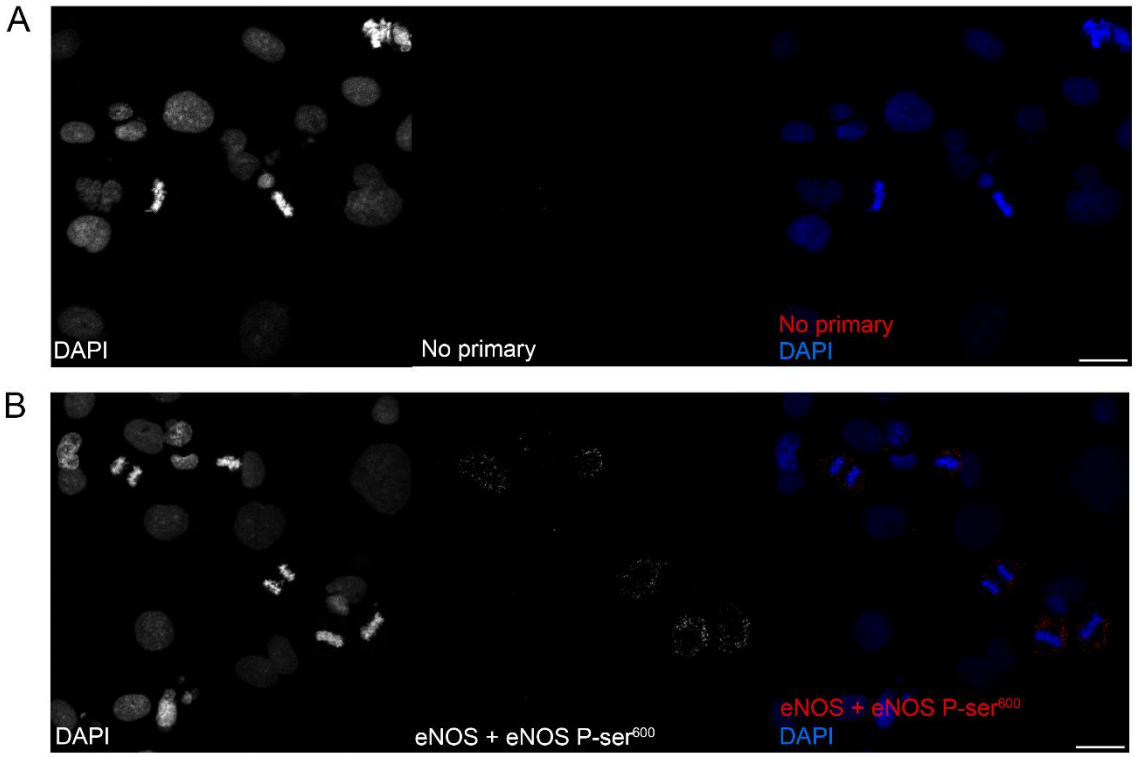

Figure 7. **Proximity ligation assay of an eNOS monoclonal antibody and the P-ser^{600} antibody.** Proximity ligation assay results using a mouse monoclonal eNOS antibody and our rabbit polyclonal eNOS ser-600 phosphorylation antibody, without primary antibodies no signal is observed (A) whereas when both antibodies are present signal is observed in mitotic cells (B). Scale bars represent 20 μm.

ser^{600} antibody alone – on the periphery of the cell. This data supports the specificity of our antibody and helps validate our previous observations with this antibody.

eNOS phosphorylated at ser^{600} is shifted by 10 kD on SDS-PAGE

Given that we can elevate the amount of P-ser^{600} observed by synchronizing cells at the G2/M barrier, we wanted to collect semi-quantitative data using western blot analysis. We confirmed our finding that eNOS phosphorylated at ser^{600} is elevated around 30-60 minutes after entrance into mitosis, and observed, under our western conditions, that the P-ser^{600} antibody reacts with a band that is shifted by 10 kD when compared to eNOS reactivity using several eNOS antibodies. We observe reactivity of the mouse monoclonal eNOS antibody at approximately 140 kD whereas the P-ser^{600} antibody is reacting roughly 10 kD higher at approximately 150 kD (figure 8). It is worth noting that the eNOS antibody does not also react with the 150 kD band unless we significantly increase the input. This suggests that an amount of eNOS that can react with eNOS antibody is not present in the heavier band and likely means that a smaller amount of eNOS is present at the heavier band. Interestingly, reaction to a P-ser^{1177} antibody, which has an epitope that could overlap

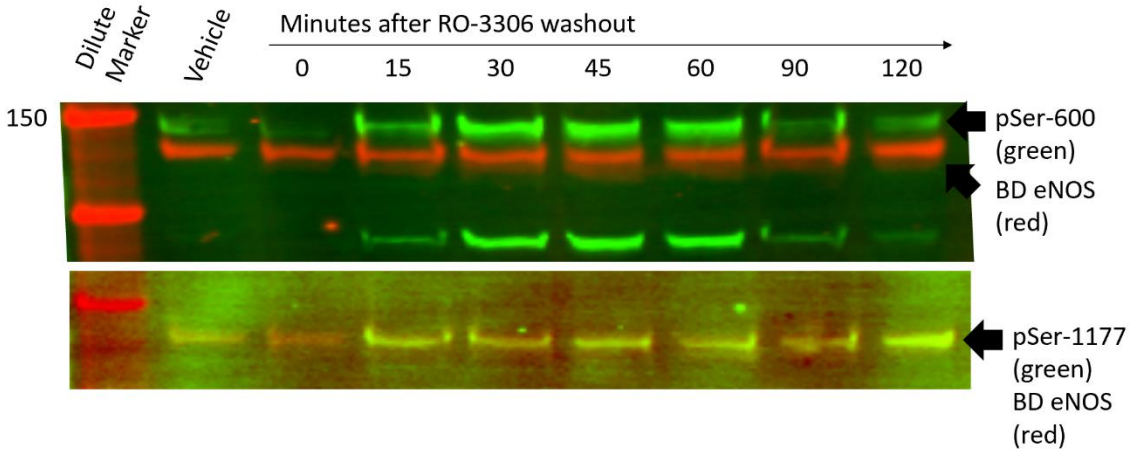

Figure 8. **eNOS P-ser^{600} is shifted by 10 kD on western blots.** Western blot analysis shows that eNOS P-ser^{600} is shifted by roughly 10 kD heavier than eNOS. Comparatively, eNOS modified by other phosphorylation, including P-ser^{1177} is not shifted and has reactivity that overlaps with the eNOS antibody.

with the eNOS antibody used in this blot. Together, this suggests that P-ser^{600} may be co-posttranslationally modified with a modification of roughly 10 kD.

Other eNOS phosphorylation sites are not changing significantly after RO-3306 washout

Using the same methodology to assess P-ser^{600} with western blotting, we investigated other commonly studied phosphorylation sites on eNOS. We found that phosphorylation at ser^{1177} is slightly elevated in cells at 15-120 minutes after RO-3306 washout when compared to the vehicle control and 0-minute (G2/M block intact) time point. However, when compared to the degree of modulation of P-ser^{600}, the change in P-ser^{1177} and P- ser^{635} is minimally elevated compared to the vehicle treated cells. Additionally, other sites like, ser^{114} and thr^{495} do not seem to be changing throughout the time course (figure 9). It is worth noting that we did not explore phosphorylation of tyr residues with our western blots which may be worth a brief investigation.

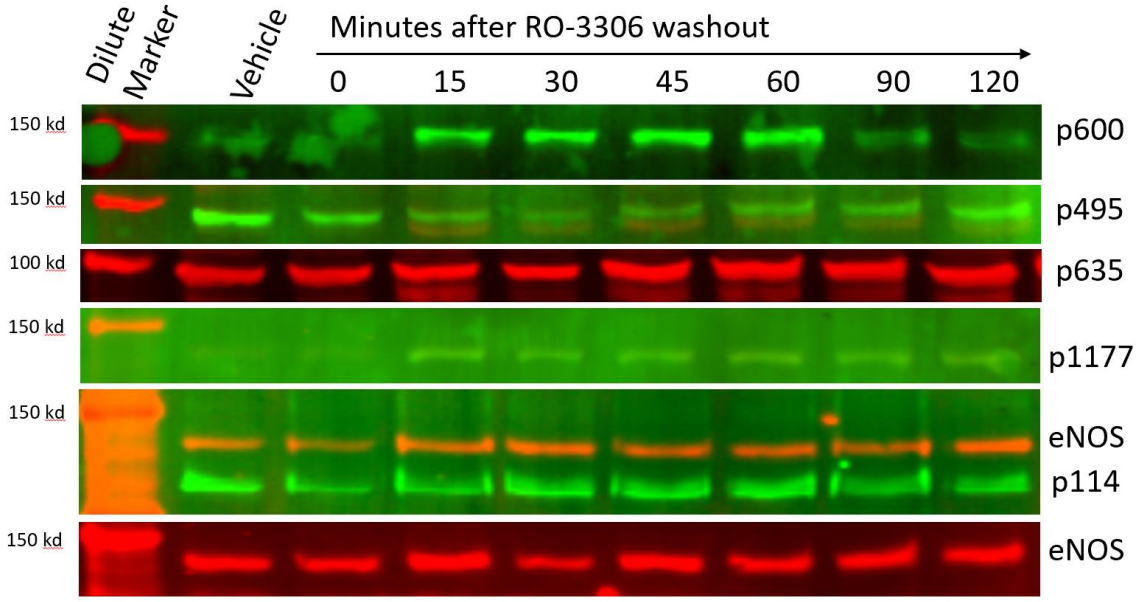

Figure 9. **Western blot analysis of phosphorylation of other eNOS sites.** Representative western blot of two independent experiments showing phosphorylation status of multiple eNOS phosphorylation sites following RO-3306 washout.

MAPK activation does not correspond to the increase in eNOS P-ser^{600}

Previous data from our lab showed that eNOS can be phosphorylated by MAPKs. Specifically, eNOS is phosphorylated by ERK, JNK, and p38. Where JNK phosphorylates at ser^{114}, ERK phosphorylates at ser^{600}, and p38 phosphorylates both sites (supplemental figure 2). It is worth noting that MAPK phosphorylation was used as a measure of kinase activity and that ideally, a substrate should be looked at to ensure activity. All three MAPKs seem to be phosphorylated significantly at 15 minutes into the washout when compared to the vehicle or 0-minute time point (figure 10). At first glance, this seems to match up with the increase in eNOS P-ser^{600}, but this does not appear to be entirely the case. P38 phosphorylation decreases by 30 minutes into the time course which makes it unlikely to be the cause of peak P-ser^{600} at around 45 minutes (figure 10). JNK is unable to phosphorylate eNOS at ser^{600} *in vitro* (supplemental figure 2). ERK maintains the activation phosphorylation sites for the entire time frame which makes ERK more likely to enhance P-ser^{600}, however, the ERK phosphorylation lasts significantly longer than ser^{600} phosphorylation (figure 10).

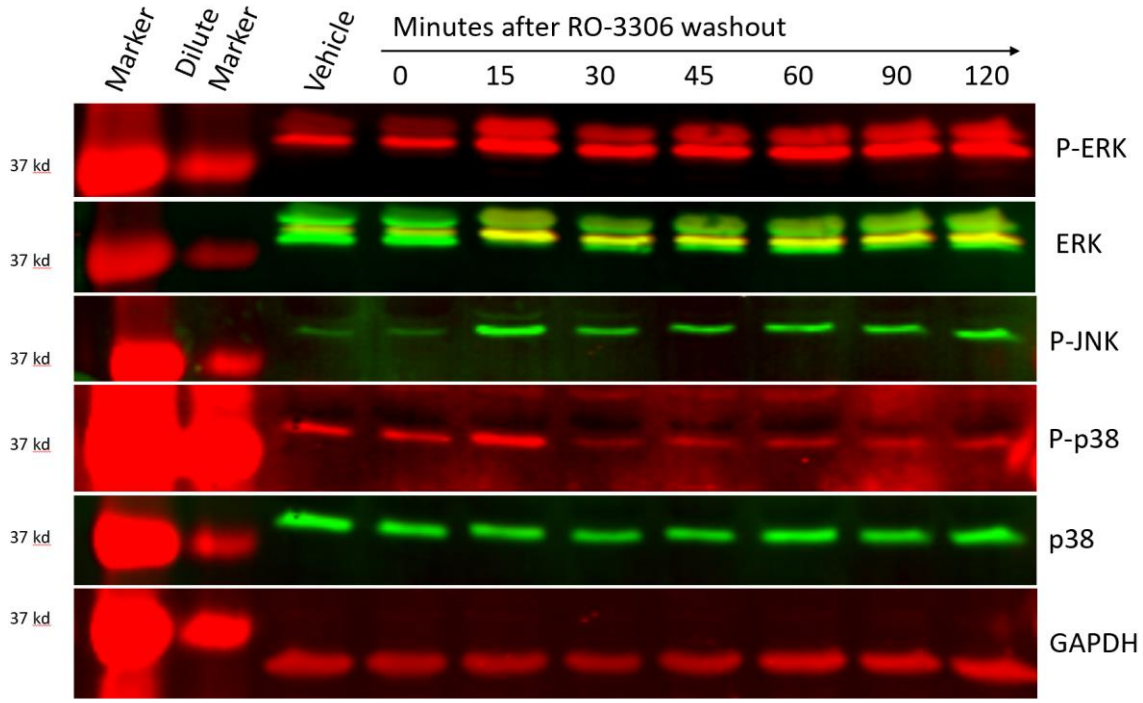

Figure 10. **Western blot analysis of MAPKs**. Representative western blot of two independent experiments showing changes in MAPK phosphorylation following RO-3306 washout.

CHAPTER 4 – DISCUSSION

In order to assess the possible significance of eNOS ser^{600} phosphorylation, we created a multiple sequence alignment to verify that more than just humans and cows have this phosphorylation site. The eNOS protein sequence alignment shows us that there is high conservation throughout most of the primary and secondary protein structure of eNOS (figure 1). We also found that all phosphorylation sites that influence activity are conserved across taxonomical classes in our data set. Our data matches observations in a detailed study on the phylogeny of NOS enzymes by Andreakis et al. However, it is still worth mentioning that our data set is limited to a blast search using the protein sequence of eNOS.

Our study found that ser^{600} occurs exclusively in mammals and marsupials in our data set. This suggests that as part of the evolutionary differentiation from reptiles and aves, this site appeared in mammals. One possible explanation for the appearance of this site may correspond with the branch that distinguishes cold-blooded animals from warm-blooded animals. Our data suggests that ser^{600} may have been a more recent mutation in eNOS which aligns with the phylogenetic analysis of NOS enzymes by Andreakis et al (34). That study identifies eNOS as the last NOS enzyme to appear in organisms. However, as there is limited data in the literature on this site in other species outside of cows, further work is necessary before significant conclusions can be made on the evolutionary significance of ser^{600}.

Using the same sequence alignment, we found that all phosphorylation sites that alter NO production by eNOS were conserved in our data set. However, ser^{114} and ser^{600} were only found in sequences from warm blooded animals in our study. We believe that these sites do not directly influence NO production of eNOS by perturbing electron

transport, but rather, influence eNOS binding partners which may contribute to the ambiguity in activity differences observed in the literature (39). Another observation stems from a conserved phosphorylation site between tyr^{657} on eNOS and tyr^{895} on nNOS. Phosphorylation at this site has inverse effects between the two NOS enzymes where on eNOS it inhibits activity, but on nNOS it enhances activity. This likely results from other differences found on the nearby AIL. In nNOS, the region has fewer hydrophobic residues than eNOS. Additionally, there is a WRKRRK portion on eNOS this is absent from nNOS. We have proposed that this motif is a MAPK binding site (24). Therefore, eNOS may be more heavily regulated by MAPKs via the AIL. However, in order to make strong conclusions, a structural model of the AIL is necessary. While parts of eNOS and other NOSs have resolved structural information, the AIL has not been elucidated for both enzymes, therefore it is difficult to attribute differences in activity solely on differences in the primary structure.

The AIL has not been fully elucidated structurally. However, due to the partial homology in primary sequence and high conservation of structural elements between NOS enzyme structures we were able to create a threaded model using the structure of human iNOS bound to calmodulin (PDB 3HR4). Specifically, we used the flavodoxin-like domain as our template for the model because of the high structural conservation between eNOS and iNOS which includes multiple alpha helices and beta strands that can act as anchor points. Three sites found on the AIL have been published to directly influence eNOS activity in the literature ser^{615}, ser^{633}, and tyr^{657} (none shown in figure 2). Of these sites, tyr^{657} has been structurally resolved in multiple reported NOS structures and is found in the FMN binding site which explains how phosphorylation could sterically hinder FMN

binding and cause the reported inhibitory effect (40). The other serine sites known to influence eNOS activity are more likely to be near the FMN bound to eNOS acting to enhance electron transport. However, since these sites are not fully elucidated structurally, exact positions in the structure of eNOS are not entirely known. One site that is also found in the AIL is ser^{600}, this site is near the base of a helix that is completely resolved and involved in the FMN binding domain of the flavodoxin-like domain of eNOS (shown in purple in figure 2). This makes it more likely that ser^{600} is more not influencing activity due to the distance from the FMN. However, phosphorylation at ser^{600} could influence eNOS binding partners resulting in an indirect activity changes or changes in subcellular localization.

In testing our phosphospecific ser^{600} antibody, we observed a significantly elevated level of staining in rounded cells that were partially detached from the slide. At first, we thought this staining was identifying cells undergoing apoptosis, but after closer inspection, it appeared that the DNA was not fragmenting but rather condensing like at the start of mitosis. This was verified using flow cytometry and looking at DNA density where we observe a small population of P-ser^{600} elevated cells that corresponds to the percentage of cells that could be in mitosis in an asynchronous population. The DNA staining matched with N=4 DNA suggesting late cell cycle cells are P-ser^{600} elevated (figure 3). Additionally, we were able to increase the population of P-ser^{600} using a CDK 1 inhibitor – RO-3306 – to synchronize cells at the G2/M checkpoint (figure 4). This inhibitor is reversible and therefore should minimally interact with other kinases, but nonetheless it has been reported to interact with PKC gamma and serum/glucocorticoid-regulated kinase (SGK) with a Ki (nM) of 318 and 497 respectively. Other kinases that have been shown to phosphorylate

eNOS such as, ERK, PKA, and AKT had an approximately 2000 nM Ki or greater (41). Ultimately, we believe that the inhibitor itself is not directly impacting levels P-ser^{600} and is acting as a cell synchronization agent in our conditions. Therefore, by using cell synchronization and immunofluorescence costaining we observed that P-ser^{600} is elevated during mitosis. We further verified this direct link between P-ser^{600} and mitosis by detecting histone H3 ser^{28} phosphorylation which is a mitotic indicator (42). Additionally, DNA density staining also supports our interpretation. Ultimately, our data supports the notation that P-ser^{600} is enhanced during mitosis.

In order to ensure that changes in P-ser^{600} are not from changing eNOS levels, we employed both immunofluorescence and flow cytometry. This showed that asynchronous cells maintain a similar amount of eNOS (figure 5) throughout the cell cycle. When comparing our data with the literature, we found that eNOS does not significantly change throughout the cell cycle (43). Therefore, we believe that P-ser^{600} is not elevated due rising eNOS levels. However, because our study relies on an antibody to P-ser^{600} with limited reported data, we wanted to verify specificity of the antibody. We did this by using a proximity ligation assay which produces signal only if two antibodies are within 40 nm. This highly specific assay was employed with a mouse monoclonal antibody to eNOS and our rabbit anti-P-ser^{600} antibody. This produced a similar signal to what is observed with immunostaining of P-ser^{600}, therefore we conclude that our antibody is specific to eNOS (figure 6). Additionally, we immunoprecipitated with the P-ser^{600} antibody, collected the main band around 150 kD, and submitted for mass spectrometry. After a trypsin digestion, we observed fragments of eNOS protein in our sample (supplemental figure 4). We have also previously reported that the antibody signal is ablated when treating lysates with

lambda phosphatase and antibody signal is elevated when eNOS is incubated with ERK (24). Taken together, this suggests that our antibody is specific to eNOS that is phosphorylated at ser^{600}.

Our study also found significant elevation in P-ser^{600} through western blotting by collecting cell lysates different time points following release of the G2/M block by RO-3306. Interestingly, eNOS that was phosphorylated at ser^{600} was shifted by 10 kD in our conditions (figure 7). We hypothesize that this shift is the result of some posttranslational modification that is approximately 10 kD. We also observe a slight, but nonetheless significant elevation in P-ser^{1177} (figure 8). Gentile et al. has observed that P-ser^{1177} is elevated in mouse embryonic endothelial cells when stimulated with VEGF as part of angiogenesis in embryonic development (32). Similarly, our data supports that dividing microvascular endothelial cells have an increase in P-ser^{1177}. This is likely also associated with angiogenesis mechanisms for formation of new capillaries. However, when comparing our data with quercetin induced mitotic arrest of bovine aortic endothelial cells, we do not observe the same modulation in eNOS phosphorylation sites (44). Jackson et al. found that P-ser^{114} and P-ser^{615} are decreased with increasing amounts of mitotic arrest. Also, Jackson et al. found that P-ser^{1177} and P-thr^{495} were consistent regardless of degree of mitotic arrest. However, under our conditions, we observed consistent levels of P-ser^{114} phosphorylation, decreasing P-thr^{495}, and increasing P-ser^{1177}. This raises the possibility that there may be significantly different mechanisms governing the regulation of eNOS phosphorylation between microvasculature and macrovasculature during cellular division.

We previously reported that ERK can phosphorylate eNOS at ser^{600} *in vitro* (24). Here we show that *in situ* phosphorylation of ser^{600} is likely not caused by a MAPK. We

found that elevation of P-ser^{600} does not correspond to elevations in MAPK activation phosphorylation (figure 9). We found that JNK is unable to phosphorylate at ser^{600} *in vitro* and is highly unlikely to phosphorylate *in situ* (supplemental figure 2). Additionally, we found that p38 can phosphorylate at ser^{600} but the phosphorylation of p38 in our time course does not correspond to changes in P-ser^{600}. ERK was thought to be the physiological kinases responsible for P-ser^{600}, but the EGF in the media stimulated cells for greater than 2 hours, which does not correspond to the elevation in P-ser^{600}. Together, this rules out JNK and p38 as the physiological kinase responsible for the phosphorylation in our conditions. Therefore, we suggest that an EGF independent mechanism of ERK activation may still be responsible for the elevated P-ser^{600}, but further work is necessary before strong conclusions can be made. Additionally, we did *in vitro* kinase activity assays with eNOS and CDK 1/cyclin B, CDK 2/cyclin E, and CDK 5/p25. We found that CDK 2 and CDK 5 are both able to phosphorylate at ser^{600} (supplementary figure 3). Together this tells us that a CDK could be responsible for the phosphorylation event, but ultimately further research is necessary to elucidate the kinase responsible for P-ser^{600}.

CHAPTER 5 – CONCLUSIONS AND FUTURE DIRECTIONS

All together our study has found that ser^{600} phosphorylation is modulated during late cell cycle and at the start of mitosis. Additionally, this phosphorylation event is not attributed to an increase in overall eNOS protein levels. We were able to verify this through multiple experimental methods ranging from immunofluorescence, flow cytometry and western blotting. Additionally, we have verified that our P-ser^{600} antibody is specific to eNOS that is phosphorylated at ser^{600} which helps provide additional data to the limited data available on this antibody. We have attempted to also distinguish which kinases are responsible for the P-ser^{600}. This resulted in ruling out p38 and JNK for the P-ser^{600} at the start of mitosis and found that ERK could be responsible in what would be hypothesized to be an EGFR independent mechanism, but ultimately further work is necessary to make stronger conclusions about ERK involvement in ser^{600} phosphorylation. Additionally, we found that eNOS is shifted by 10 kD on gels when it is phosphorylated at ser^{600} which suggests that another posttranslational modification on eNOS is occurring, one which causes this 10 kD shift. Even more interestingly, we found that eNOS phosphorylated at ser^{600} is found in a unique distribution pattern within cells, but this also needs additionally research before a stronger conclusion can be made. Taken together, we have presented data that shows that ser^{600} is phosphorylated in tissue culture and its modulation in a cell cycle dependent manner. This work should be replicated using animal models in order to fully understand the significance of ser^{600} in the context of the cardiovascular system.

One possible explanation for the role of ser^{600} phosphorylation physiologically could be through migration. Our lab had found that CDK 5 is capable of phosphorylating at ser^{600}. Recently, Lampropoulou et al. found that CDK 5 is involved in endothelial cell

migration as part of pleiotrophin agonized mechanism. Pleiotrophin is a hypothesized angiogenic growth factor that is binds with strong affinity to heparin receptors (45). Together this suggests that a potential physiological roll for eNOS ser^{600} phosphorylation could be participation in migration. While ser^{600} phosphorylation directly does not seem to influence NO output, when coupled with phosphorylation by an activating kinase, protein kinase A (PKA), eNOS output is significantly greater than with PKA incubation alone (data not shown). Additionally, it appears that ser^{600} phosphorylation in immunofluorescence shows a unique staining pattern like what is observed when staining with intermediate filaments suggesting a cytoskeletal specific distribution. The cause of the distribution is unknown, but we believe that the phosphorylation at ser^{600} in conjunction with the additional modification resulting in the observed 10 kD shift on SDS-PAGE could together result in the unique staining. The increased NO output by eNOS could be the mechanism used to break down these cytoskeletal elements as part of the pleiotrophin induced CDK 5 mediated endothelial cell migration observed by Lampropoulou (46). One way to test this would be by using the method described by Ni et al. to immortalize microvascular endothelial cells from mice. So long as the original eNOS promoter is not changed as part of the knockout, theoretically, we could introduce a plasmid with that promoter and the sequence of eNOS with mutations at residues of eNOS we are interested in without the worry of dealing with the wild type population of eNOS that would be present in simple transfection experiments with other endothelial cells. It would be interesting to investigate the role of ser^{600} on endothelial cell migration using this model system. Additionally, if the other posttranslational modification we believe is associated with ser^{600} phosphorylation is found to be a mono ubiquitin-like modification (approximately 8 kD and includes protein

like ubiquitin, small ubiquitin-like modifier (SUMO) proteins, or NEDD8), then we could theoretically mutate the lysine residue to a arginine residue which would be unable to be modified. This could result in different physiological changes, but we believe the most likely observation from this set of experiments would be a change in the subcellular distribution of ser^{600} phosphorylated eNOS from localization at intermediate filaments to a cytoplasmic distribution. Additionally, the physiological role of NO in migration could be perturbed and the rate of migration for cells without the lysine modification could be much slower as cytoskeletal intermediate filaments may not be broken down as efficiently as the wild type eNOS. This is one possible explanation for the role of ser^{600} phosphorylation, ultimately, a significant amount of work is necessary before stronger conclusions can be made.

One interesting route of investigation would be to look at differences in ser^{600} phosphorylation between male-derived compared to female-derived endothelial cells. Recently, Cattaneo et al. identified that differences in eNOS expression and function between male-derived and female-derived endothelial cells (42). This group found that eNOS expression is twice as high in female endothelial cells compared to male endothelial cells. Additionally, they found that the mechanisms surrounding endothelial functions like migration was sex specific. For example, they observed that male endothelial cells use an eNOS independent and cellular proliferation-based mechanism for wound recovery whereas female endothelial cells use an eNOS dependent and cellular proliferation independent mechanism. To elaborate, female endothelial cells rely on eNOS to assist in recovering from wounding and do not simply just divide to fill the wounded area like male endothelial cells. As part of this mechanism, female endothelial cells get larger than male

endothelial cells. With the differences in wound recovery in mind, due to the mitotic nature of ser^{600} phosphorylation, we believe that male endothelial cells would express elevated levels of P-ser^{600} as part of wound recovery and this would not be observed in female endothelial cells due to the proliferation-independent mechanism governing wound recovery. This could be the result of differences in gene expression where the network of genes guiding wound healing are sex specific. However, if P-ser^{600} is also associated with a role in breaking down the cellular cytoskeleton, then elevation may also be observed in female endothelial cells as intermediate filaments are broken down with enhanced production of NO. Ultimately, over 6,500 protein-coding genes have been found to have differential expression in adults based on sex (47). This opens the possibility of sex-specific regulatory elements which could result in totally different regulation mechanisms between males and females. Ultimately, further research is necessary in order to determine the influence that sex-specific gene networks have on NOS regulation.

Another route of investigation could be on the regulatory differences between the microvasculature and macrovasculature. It is well established that the endothelial phenotype differs slightly based on the vascular bed the endothelial cells are associated with (48). Despite many physiologically similar functions, endothelial cells are different segmentally. For example, phenotypically, arterial endothelial cells are different than capillary endothelial cells which are different than venous endothelial cells. There are two major classes of endothelium, microvascular and macrovascular. There is ambiguity in the literature with regards to endothelial functional differences between these two types of endothelium where some researchers report finding an association between micro- and macrovasculature and others do not (49-51). This suggests that the underlying mechanism

may be organ specific and varies by disease. Additionally, it is important to note that the single layer of endothelium surrounds other organs besides the interior of blood vessels and is inherently difficult to isolate and study. However, this leaves open the possibility that endothelium associated with different organs may be regulated differentially. It would be worth studying the regulatory differences that result in the ambiguity in the literature regarding the functional association between microvasculature and macrovasculature. Specifically, it would be interesting in the context of phosphorylation regulation during mitotic events associated with wound recovery and angiogenesis. As well as, the role of eNOS ser^{600} phosphorylation in these conditions. Ultimately, due to limited amount of data available in the literature with regards to ser^{600}, significantly more research is necessary before any conclusions can be made with confidence.

REFERENCES

1. Ignarro LJ, Buga GM, Wood KS, Byrns RE, Chaudhuri G. Endothelium-derived relaxing factor produced and released from artery and vein is nitric oxide. *Proc Natl Acad Sci U S A*. 1987;84(24):9265–9269. doi:10.1073/pnas.84.24.9265
2. Villalobo A. REVIEW ARTICLE: Nitric oxide and cell proliferation. FEBS Journal. 2006;273(11):2329-2344. doi:10.1111/j.1742-4658.2006.05250.x
3. Sessa WC. eNOS at a glance. Journal of Cell Science. 2004;117(12):2427-2429. doi:10.1242/jcs.01165
4. To NO or not to NO: “where”? is the question. Histology and Histopathology. 2004;(19):585-605. doi:10.14670/HH-19.585
5. Ying L, Hofseth LJ. An Emerging Role for Endothelial Nitric Oxide Synthase in Chronic Inflammation and Cancer. Cancer Research. 2007;67(4):1407-1410. doi:10.1158/0008-5472.can-06-2149
6. Li H, Förstermann U. Nitric oxide in the pathogenesis of vascular disease. The Journal of Pathology. 2000;190(3):244-254. doi:10.1002/(sici)1096-9896(200002)190:3<244::aid-path575>3.0.co;2-8
7. Luiking YC, Engelen MP, Deutz NE. Regulation of nitric oxide production in health and disease. Current Opinion in Clinical Nutrition and Metabolic Care. 2010;13(1):97-104. doi:10.1097/mco.0b013e328332f99d
8. Phaniendra A, Jestadi DB, Periyasamy L. Free radicals: properties, sources, targets, and their implication in various diseases. Indian J Clin Biochem. 2015;30(1):11–26. doi:10.1007/s12291-014-0446-0
9. Epstein FH, Moncada S, Higgs A. The L-Arginine-Nitric Oxide Pathway. *N Engl J Med*. 1993;329(27):2002-2012. doi:10.1056/NEJM199312303292706
10. Förstermann U, Sessa WC. Nitric oxide synthases: regulation and function. *Eur Heart J*. 2012;33(7):829-837. doi:10.1093/eurheartj/ehr304
11. Baek KJ, Thiel BA, Lucas S, Stuehr DJ. Macrophage nitric oxide synthase subunits. Purification, characterization, and role of prosthetic groups and substrate in regulating their association into a dimeric enzyme. *J Biol Chem* . 1993;268(28):21120-21129.
12. Nishida CR, de Montellano PRO. Autoinhibition of Endothelial Nitric-oxide Synthase: IDENTIFICATION OF AN ELECTRON TRANSFER CONTROL ELEMENT . *J Biol Chem* . 1999;274(21):14692-14698.
13. Chan Y, Fish JE, D’Abreo C, et al. The Cell-specific Expression of Endothelial Nitric-oxide Synthase: A ROLE FOR DNA METHYLATION . *J Biol Chem* . 2004;279(33):35087-35100.

14. Huang PL, Lo EH. Chapter 2 Genetic analysis of NOS isoforms using nNOS and eNOS knockout animals. *Prog Brain Res*. 1998;118:13-25. doi:10.1016/S0079-6123(08)63197-0

15. Sessa WC, Garca-Cardea G, Liu J, et al. The Golgi Association of Endothelial Nitric Oxide Synthase Is Necessary for the Efficient Synthesis of Nitric Oxide. *J Biol Chem* . 1995;270(30):17641-17644.

16. Fulton D, Fontana J, Sowa G, et al. Localization of Endothelial Nitric-oxide Synthase Phosphorylated on Serine 1179 and Nitric Oxide in Golgi and Plasma Membrane Defines the Existence of Two Pools of Active Enzyme. *J Biol Chem* . 2002;277(6):4277-4284.

17. Fulton D, Gratton J-P, Sessa WC. Post-Translational Control of Endothelial Nitric Oxide Synthase: Why Isn't Calcium/Calmodulin Enough? *J Pharmacol Exp Ther*. 2001;299(3):818 LP-824.

18. Butt E, Bernhardt M, Smolenski A, et al. Endothelial Nitric-oxide Synthase (Type III) Is Activated and Becomes Calcium Independent upon Phosphorylation by Cyclic Nucleotide-dependent Protein Kinases. *J Biol Chem*. 2000;275(7):5179-5187.

19. Boo YC, Sorescu GP, Bauer PM, et al. Endothelial NO synthase phosphorylated at SER635 produces NO without requiring intracellular calcium increase. *Free Radic Biol Med*. 2003;35(7):729-741.

20. Mount PF, Kemp BE, Power DA. Regulation of endothelial and myocardial NO synthesis by multi-site eNOS phosphorylation. *J Mol Cell Cardiol*. 2007;42(2):271-279. doi:10.1016/j.yjmcc.2006.05.023

21. Chen F, Kumar S, Yu Y, et al. *PKC-Dependent Phosphorylation of ENOS at T495 Regulates ENOS Coupling and Endothelial Barrier Function in Response to G+ -Toxins*. Vol 9.; 2014. doi:10.1371/journal.pone.0099823

22. Ruan L, Torres CM, Buffett RJ, Kennard S, Fulton D, Venema RC. Calcineurin-mediated Dephosphorylation of eNOS at Serine 116 Affects eNOS Enzymatic Activity Indirectly by Facilitating c-Src Binding and Tyrosine 83 Phosphorylation. *Vascular pharmacology*. 2013;59(0):10.1016/j.vph.2013.05.004. doi:10.1016/j.vph.2013.05.004.

23. Ruan L, Torres CM, Qian J, et al. Pin1 Prolyl Isomerase Regulates Endothelial Nitric Oxide Synthase. *Arteriosclerosis, thrombosis, and vascular biology*. 2011;31(2):392-398. doi:10.1161/ATVBAHA.110.213181.

24. Salerno JC, Ghosh DK, Razdan R, et al. Endothelial nitric oxide synthase is regulated by ERK phosphorylation at Ser^{602}. *Bioscience Reports*. 2014;34(5):e00137. doi:10.1042/BSR20140015.

25. Fulton D, Church JE, Ruan L, et al. Src Kinase Activates Endothelial Nitric-oxide Synthase by Phosphorylating Tyr-83. *J Biol Chem*. 2005;280(43):35943-35952.

26. Fulton D, Ruan L, Sood SG, Li C, Zhang Q, Venema RC. Agonist-stimulated endothelial nitric oxide synthase activation and vascular relaxation. Role of eNOS phosphorylation at Tyr83. *Circ Res*. 2008;102(4):497-504. doi:10.1161/circresaha.107.162933

27. Loot AE, Schreiber JG, Fisslthaler B, Fleming I. Angiotensin II impairs endothelial function via tyrosine phosphorylation of the endothelial nitric oxide synthase. *The Journal of Experimental Medicine*. 2009;206(13):2889-2896. doi:10.1084/jem.20090449.

28. Dai X, Faber JE. Endothelial Nitric Oxide Synthase Deficiency Causes Collateral Vessel Rarefaction and Impairs Activation of a Cell Cycle Gene Network During Arteriogenesis. *Circulation Research*. 2010;106(12):1870-1881. doi:10.1161/CIRCRESAHA.109.212746.

29. Sharma R V, Tan E, Fang S, Gurjar M V, Bhalla RC. NOS gene transfer inhibits expression of cell cycle regulatory molecules in vascular smooth muscle cells. *Am J Physiol Circ Physiol*. 1999;276(5):H1450-H1459. doi:10.1152/ajpheart.1999.276.5.H1450

30. Lee C-H, Wei Y-W, Huang Y-T, et al. CDK5 phosphorylates eNOS at Ser-113 and regulates NO production. *J Cell Biochem*. 2010;110(1):112-117. doi:10.1002/jcb.22515

31. Cho D-H, Seo J, Park J-H, et al. Cyclin-dependent kinase 5 phosphorylates endothelial nitric oxide synthase at serine 116. *Hypertens (Dallas, Tex 1979)*. 2010;55(2):345-352. doi:10.1161/hypertensionaha.109.140210

32. Gentile C, Muise-Helmericks RC, Drake CJ. VEGF-mediated phosphorylation of eNOS regulates angioblasts and embryonic endothelial cell proliferation. *Developmental biology*. 2013;373(1):163-175. doi:10.1016/j.ydbio.2012.10.020.

33. Schleicher M, Brundin F, Gross S, Müller-Esterl W, Oess S. Cell Cycle-Regulated Inactivation of Endothelial NO Synthase through NOSIP-Dependent Targeting to the Cytoskeleton. *Molecular and Cellular Biology*. 2005;25(18):8251-8258. doi:10.1128/MCB.25.18.8251-8258.2005.

34. Andreakis N, D'Aniello S, Albalat R, et al. Evolution of the Nitric Oxide Synthase Family in Metazoans. Molecular Biology and Evolution. 2010;28(1):163-179. doi:10.1093/molbev/msq179

35. Xia C, Misra I, Iyanagi T, Kim JJ. Regulation of interdomain interactions by calmodulin in inducible nitric-oxide synthase. J Biol Chem. 2009;284(44):30708–30717. doi:10.1074/jbc.M109.031682

36. Garcin ED, Bruns CM, Lloyd SJ, et al. Structural Basis for Isozyme-specific Regulation of Electron Transfer in Nitric-oxide Synthase. Journal of Biological Chemistry. 2004;279(36):37918-37927. doi:10.1074/jbc.m406204200

37. Volkmann N, Martásek P, Roman LJ, et al. Holoenzyme structures of endothelial nitric oxide synthase - an allosteric role for calmodulin in pivoting the FMN domain for electron transfer. *J Struct Biol*. 2014;188(1):46–54. doi:10.1016/j.jsb.2014.08.006

38. Söderberg O, Gullberg M, Jarvius M, et al. Direct observation of individual endogenous protein complexes in situ by proximity ligation. Nature Methods. 2006;3(12):995-1000. doi:10.1038/nmeth947

39. Heiss EH, Dirsch VM. Regulation of eNOS enzyme activity by posttranslational modification. Curr Pharm Des. 2014;20(22):3503–3513.

40. Fisslthaler B, Loot AE, Mohamed A, Busse R, Fleming I. Inhibition of Endothelial Nitric Oxide Synthase Activity by Proline-Rich Tyrosine Kinase 2 in Response to Fluid Shear Stress and Insulin. Circulation Research. 2008;102(12):1520-1528. doi:10.1161/circresaha.108.172072

41. Vassilev LT, Tovar C, Chen S, et al. Selective small-molecule inhibitor reveals critical mitotic functions of human CDK1. Proc Natl Acad Sci U S A. 2006;103(28):10660–10665. doi:10.1073/pnas.0600447103

42. Sawicka A, Seiser C. Histone H3 phosphorylation - a versatile chromatin modification for different occasions. Biochimie. 2012;94(11):2193–2201. doi:10.1016/j.biochi.2012.04.018

43. Cattaneo MG, Vanetti C, Decimo I, et al. Sex-specific eNOS activity and function in human endothelial cells. Sci Rep. 2017;7(1):9612. Published 2017 Aug 29. doi:10.1038/s41598-017-10139-x

44. Jackson SJT, Venema RC. Quercetin Inhibits eNOS, Microtubule Polymerization, and Mitotic Progression in Bovine Aortic Endothelial Cells. The Journal of Nutrition. 2006;136(5):1178-1184. doi:10.1093/jn/136.5.1178

45. Kadomatsu K. Midkine and pleiotrophin in neural development and cancer. Cancer Letters. 2004;204(2):127-143. doi:10.1016/s0304-3835(03)00450-6

46. Lampropoulou E, Logoviti I, Koutsioumpa M, et al. Cyclin-dependent kinase 5 mediates pleiotrophin-induced endothelial cell migration. Scientific Reports. 2018;8(1). doi:10.1038/s41598-018-24326-x

47. Gershoni M, Pietrokovski S. The landscape of sex-differential transcriptome and its consequent selection in human adults. BMC Biol. 2017;15(1):7. Published 2017 Feb 7. doi:10.1186/s12915-017-0352-z

48. Ghitescu L, Robert M. Diversity in unity: The biochemical composition of the endothelial cell surface varies between the vascular beds. Microscopy Research and Technique. 2002;57(5):381-389. doi:10.1002/jemt.10091

49. Hansell J, Henareh L, Agewall S, Norman M. Non-invasive assessment of endothelial function - relation between vasodilatory responses in skin

microcirculation and brachial artery. Clinical Physiology and Functional Imaging. 2004;24(6):317-322. doi:10.1111/j.1475-097x.2004.00575.x

50. Eskurza I, Seals DR, DeSouza CA, Tanaka H. Pharmacologic versus flow-mediated assessments of peripheral vascular endothelial vasodilatory function in humans. The American Journal of Cardiology. 2001;88(9):1067-1069. doi:10.1016/s0002-9149(01)01997-x

51. Sandoo A, Carroll D, Metsios GS, Kitas GD, Veldhuijzen van Zanten JJ. The association between microvascular and macrovascular endothelial function in patients with rheumatoid arthritis: a cross-sectional study. *Arthritis Res Ther*. 2011;13(3):R99. Published 2011 Jun 21. doi:10.1186/ar3374

SUPPLEMENTARY INFORMATION

Supplementary Figure 1

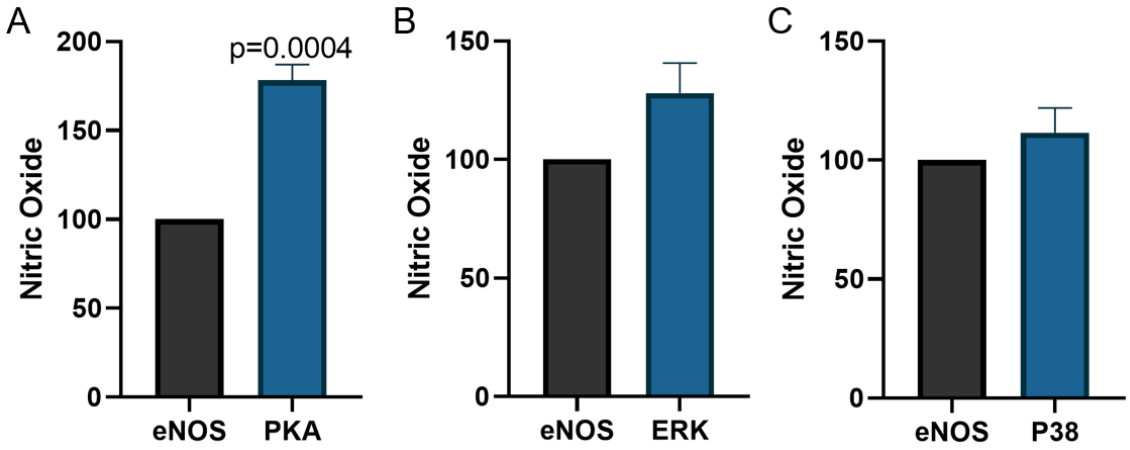

Phosphorylation of eNOS at ser^{600} and ser^{114} does not significantly alter NO production *in vitro*. Phosphorylation of eNOS with a kinase that phosphorylates at activating serine sites results in significant enhancement of NO production (A). Phosphorylation at ser^{600} by ERK and phosphorylation at ser^{114} and ser^{600} by p38 does not significantly alter NO production (B and C respectively). Data from Xzaviar Solone.

Supplementary Figure 2

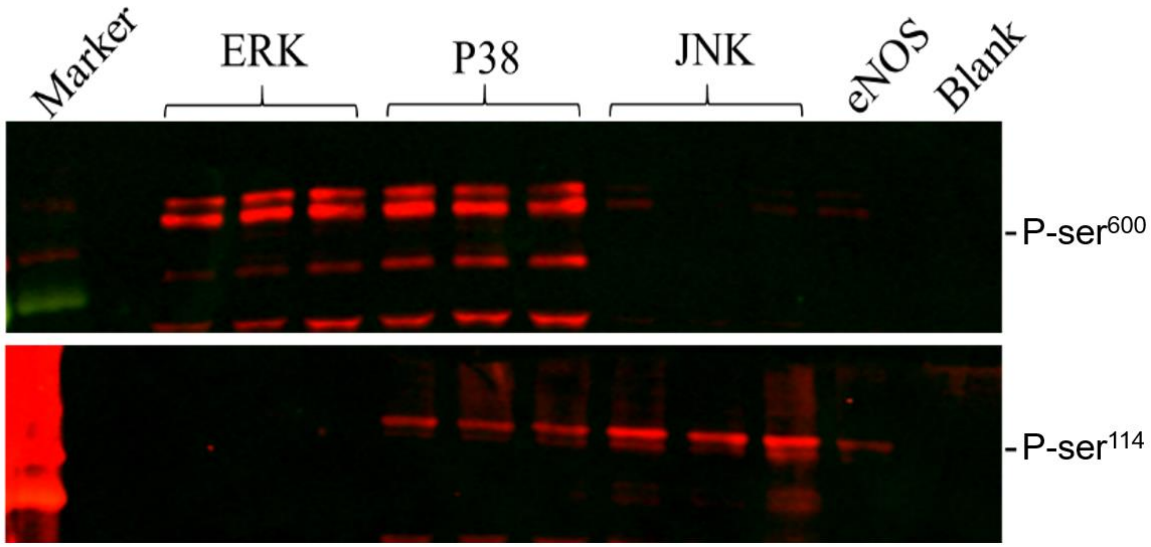

MAPKs differentially phosphorylate eNOS ser-pro sites. ERK can phosphorylate eNOS at ser^{600} but not at ser^{114}. JNK can phosphorylate at ser^{114} but not at ser^{600}. P38 can phosphorylate at both ser^{600} and ser^{114}. Data from Xzaviar Solone.

Supplementary Figure 3

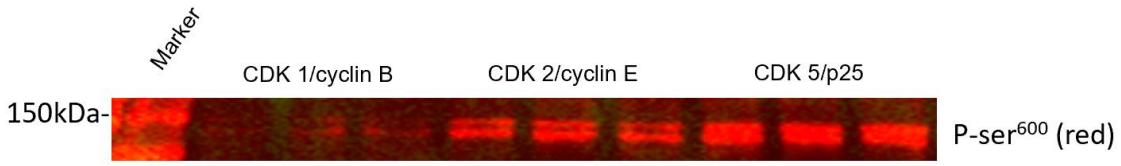

***In vitro* kinase assay with CDK 1/cyclin B, CDK 2/cyclin E, and CDK 5/p25.** 2.2uM eNOS was incubated with CDK-1 for 50 minutes and CDK-2 and CDK-5 for 30 minutes. We observe that CDK 1 does not significantly phosphorylate eNOS at ser^{600} when compared to either CDK 2 or CDK 5. It should be noted that CDK 1 is significantly less active than CDK 2 and CDK 5. Data from Xzaviar Solone.

Supplementary Figure 4

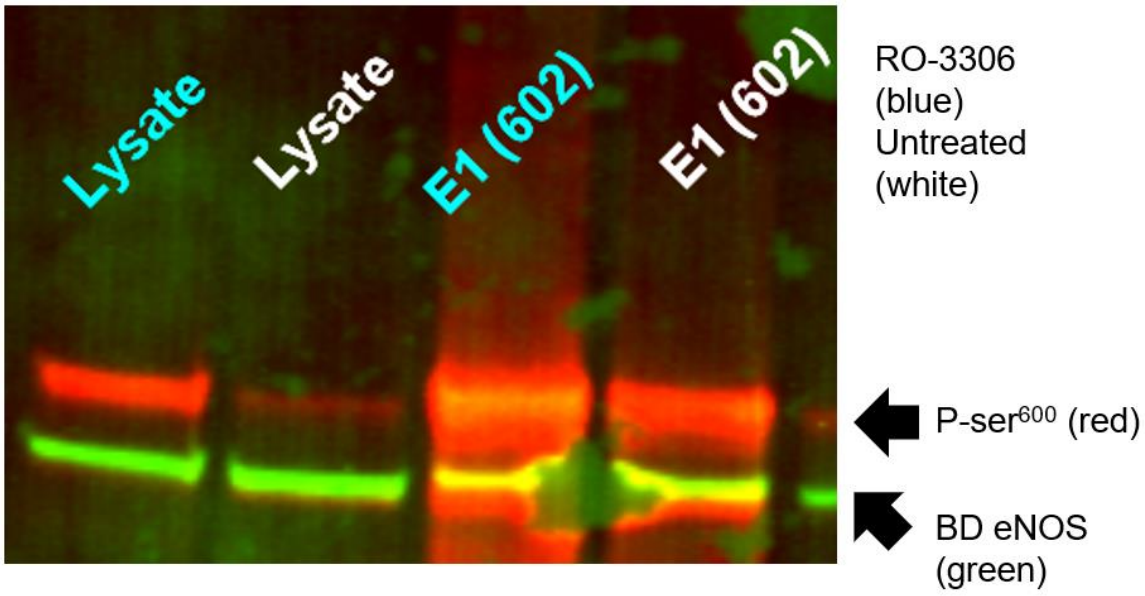

Mass spectrometry of eNOS after immunoprecipitation with anti-P-ser^{600} antibody	
Protein Sequence	**eNOS Position**
[R].CLGSLVFPR.[K]	99-107
[R].DFINQYYSSIK.[R]	129-139
[R].SAITVFPQR.[SC]	226-234
[R].IWNSQLVR.[Y]	243-250
[R].FNSISCSDPLVSSWR.[R]	613-627
[K].ESSNTDSAGALGTLR.[F]	632-646
[R].LLQLGQGDELCGQEEAFR.[G]	679-696
[R].LSAQAEGLQLLPGLIHVHR.[R]	737-755
[K].GSPGGPPPGWVR.[D]	835-846
[R].LLSTLAEEPR.[E]	876-885
[R].EQQELEALSQDPR.[R]	886-898
[R].LPPDPSLPCILVGPGTGIAPFR.[G]	1001-1022
[K].TYVQDILR.[T]	1086-1093
[R].ILATEGDMELDEAGDVIGVLR.[D]	1130-1150
[R].YHEDIFGLTLR.[T]	1155-1165

Mass spectrometry of eNOS band after immunoprecipitation with our anti-P-ser^{600} antibody. Immunoprecipitation with our anti-P-ser^{600} antibody on HMEC lysates collected 45 minutes after RO-3306 washout (blue) and untreated (white). The P-ser^{600} band (red) has reactivity with BD eNOS band (green) in the first elution. (TOP of figure) It should be noted ser^{602} (in the blot above) is bovine numbering whereas ser^{600} is human numbering. Detected eNOS fragments from mass spectrometry (BOTTOM of figure). Data from Morgan Watson.

Table 3: NOS sequences used in phylogenetic study of phosphorylation sites

Uniprot identifier	Organism	Length
G1M5X2_AILME	Ailuropoda melanoleuca (Giant panda)	1208
A0A3Q0SYZ0_AMPCI	Amphilophus citrinellus (Midas cichlid) (Cichlasoma citrinellum)	1428
H9GDL4_ANOCA	Anolis carolinensis (Green anole) (American chameleon)	1126
A0A2K5EWR1_AOTNA	Aotus nancymaae (Ma's night monkey)	1203
A0A3P8QYB8_ASTCA	Astatotilapia calliptera (Eastern happy) (Chromis callipterus)	1428
A0A383YRM3_BALAS	Balaenoptera acutorostrata scammoni (North Pacific minke whale) (Balaenoptera davidsoni)	1205
A0A3Q1LSD1_BOVIN	Bos taurus (Bovine)	1205
F6VF63_CALJA	Callithrix jacchus (White-tufted-ear marmoset)	1203
A0A3Q7NHI9_CALUR	Callorhinus ursinus (Northern fur seal)	1203
S9WKR6_CAMFR	Camelus ferus (Wild bactrian camel) (Camelus bactrianus ferus)	936
F1PV05_CANLF	Canis lupus familiaris (Dog) (Canis familiaris)	1211
A0A452EGA9_CAPHI	Capra hircus (Goat)	1193
H0V302_CAVPO	Cavia porcellus (Guinea pig)	1206
A0A2K5S0Y5_CEBCA	Cebus capucinus imitator	1203
A0A2K5NCZ8_CERAT	Cercocebus atys (Sooty mangabey) (Cercocebus torquatus atys)	1205
A0A0D9R373_CHLSB	Chlorocebus sabaeus (Green monkey) (Cercopithecus sabaeus)	867
A0A2K5IDK8_COLAP	Colobus angolensis palliatus (Peters' Angolan colobus)	1205
A0A3L7HAM2_CRIGR	Cricetulus griseus (Chinese hamster) (Cricetulus barabensis griseus)	1194
A0A2Y9NEZ8_DELLE	Delphinapterus leucas (Beluga whale)	1205

A0A1S3G337_DIPOR	Dipodomys ordii (Ord's kangaroo rat)	1201
A0A2Y9K7I3_ENHLU	Enhydra lutris kenyoni	1202
F6REP3_HORSE	Equus caballus (Horse)	1204
A0A1S3AL81_ERIEU	Erinaceus europaeus (Western European hedgehog)	1012
M3WID9_FELCA	Felis catus (Cat) (Felis silvestris catus)	1202
U3JXC0_FICAL	Ficedula albicollis (Collared flycatcher) (Muscicapa albicollis)	1435
A0A091D6A0_FUKDA	Fukomys damarensis (Damaraland mole rat) (Cryptomys damarensis)	1206
V9ITD3_CHICK	Gallus gallus (Chicken)	1146
G3RKZ4_GORGO	Gorilla gorilla gorilla (Western lowland gorilla)	997
A0A3P4RQQ4_GULGU	Gulo gulo (Wolverine) (Gluton)	997
A0A3Q2VEN8_HAPBU	Haplochromis burtoni (Burton's mouthbrooder) (Chromis burtoni)	1428
A0A0N8ETM2_HETGA	Heterocephalus glaber (Naked mole rat)	1206
A0A3M0JYH6_HIRRU	Hirundo rustica	1160
NOS3_HUMAN	Homo sapiens (Human)	1203
A0A287D6H1_ICTTR	Ictidomys tridecemlineatus (Thirteen-lined ground squirrel) (Spermophilus tridecemlineatus)	1202
W5MAD9_LEPOC	Lepisosteus oculatus (Spotted gar)	1123
A0A340YEP3_LIPVE	Lipotes vexillifer (Yangtze river dolphin)	1205
G3SZA3_LOXAF	Loxodonta africana (African elephant)	1199
A0A2K5TWM8_MACFA	Macaca fascicularis (Crab-eating macaque) (Cynomolgus monkey)	1205
A0A1D5QGM1_MACMU	Macaca mulatta (Rhesus macaque)	1205
A0A2K6B252_MACNE	Macaca nemestrina (Pig-tailed macaque)	1205

A0A2K5YFH5_MANLE	Mandrillus leucophaeus (Drill) (Papio leucophaeus)	1155
A0A3P9CX80_9CICH	Maylandia zebra (zebra mbuna)	1428
A0A1U7RHA5_MESAU	Mesocricetus auratus (Golden hamster)	1202
F6S3S1_MONDO	Monodelphis domestica (Gray short-tailed opossum)	1193
NOS3_MOUSE	Mus musculus (Mouse)	1202
M3Y867_MUSPF	Mustela putorius furo (European domestic ferret) (Mustela furo)	1211
S7NFW7_MYOBR	Myotis brandtii (Brandt's bat)	1213
G1PQK0_MYOLU	Myotis lucifugus (Little brown bat)	1203
A0A2Y9HAI4_NEOSC	Neomonachus schauinslandi (Hawaiian monk seal) (Monachus schauinslandi)	1202
A0A341C675_9CETA	Neophocaena asiaeorientalis asiaeorientalis (Yangtze finless porpoise)	1205
G1QV96_NOMLE	Nomascus leucogenys (Northern white-cheeked gibbon) (Hylobates leucogenys)	1128
A0A0U1UVC9_OCHCU	Ochotona curzoniae (Black-lipped pika)	1211
A0A2U3WJA4_ODORO	Odobenus rosmarus divergens (Pacific walrus)	1207
I3JWS0_ORENI	Oreochromis niloticus (Nile tilapia) (Tilapia nilotica)	1428
D7RVB4_RABIT	Oryctolagus cuniculus (Rabbit)	1209
H0X6T1_OTOGA	Otolemur garnettii (Small-eared galago) (Garnett's greater bushbaby)	1434
Q4U3W6_SHEEP	Ovis aries (Sheep)	1205
H2QVM2_PANTR	Pan troglodytes (Chimpanzee)	1203
A0A096NXX3_PAPAN	Papio anubis (Olive baboon)	1205
A0A402FCB4_9SAUR	Paroedura picta	1074
A0A2Y9FMB5_PHYMC	Physeter macrocephalus (Sperm whale) (Physeter catodon)	1205

A0A2J8RKC7_PONAB	Pongo abelii (Sumatran orangutan) (Pongo pygmaeus abelii)	1203
A0A2K6F776_PROCO	Propithecus coquereli (Coquerel's sifaka) (Propithecus verreauxi coquereli)	994
L5K1F9_PTEAL	Pteropus alecto (Black flying fox)	1200
F1LQC7_RAT	Rattus norvegicus (Rat)	1202
A0A2K6MEG7_RHIBE	Rhinopithecus bieti (Black snub-nosed monkey) (Pygathrix bieti)	1205
A0A2K6PX93_RHIRO	Rhinopithecus roxellana (Golden snub-nosed monkey) (Pygathrix roxellana)	1205
A0A2K6SCK8_SAIBB	Saimiri boliviensis boliviensis (Bolivian squirrel monkey)	1203
A0A1W4YWX6_SCLFO	Scleropages formosus (Asian bonytongue) (Osteoglossum formosum)	1420
Q7YSG7_PIG	Sus scrofa (Pig)	1205
A0A1U7UF18_TARSY	Tarsius syrichta (Philippine tarsier)	1200
A0A2Y9DDV9_TRIMA	Trichechus manatus latirostris (Florida manatee)	1208
L9KPE7_TUPCH	Tupaia chinensis (Chinese tree shrew)	1213
A0A452SJK1_URSAM	Ursus americanus (American black bear) (Euarctos americanus)	1202
A0A3Q7TG73_URSAR	Ursus arctos horribilis	1201
A0A384BW74_URSMA	Ursus maritimus (Polar bear) (Thalarctos maritimus)	1198
A0A3Q7RVW8_VULVU	Vulpes vulpes (Red fox)	1204
Q800E5_XENLA	Xenopus laevis (African clawed frog)	1419
F6VMJ0_XENTR	Xenopus tropicalis (Western clawed frog) (Silurana tropicalis)	1144

APPENDIX

Table of Buffers and Recipes

Protocol	**Buffer**	**Recipe/Composition**
Immunofluorescence	Blocking buffer/washing buffer	5% horse serum, 0.3% Triton X-100, and 0.01% sodium azide in PBS.
Flow Cytometry	Wash buffer	0.5% BSA in PBS
	Blocking buffer	3% BSA, 0.1% Triton X-100, and 100 μg/mL RNase A in PBS.
Western Blotting	Wash buffer	In house TBST
	Blocking buffer	Prometheus OneBlock Western-FL Blocking Buffer

Table of Primary and Secondary Antibodies and Antibody Dilutions

Protocol	**Name**	**Type**	**Dilution**	**Manufacturer – catalog #**
IF	Rabbit eNOS p602 or p600	Primary	1:200	
	Rat Histone H3 s28 phospho	Primary	1:100	Abcam – ab10543
	Rabbit eNOS	Primary	1:100	Santa Cruz – SC654
	Mouse eNOS	Primary	1:100	BD - 610297
	Mouse Vimentin	Primary	1:100	Santa Cruz – SC-6260
	Donkey anti-Mouse 555	Secondary	1:500	Invitrogen - A32773
	Goat anti-Rabbit 488	Secondary	1:250	Invitrogen - A-11034
	Donkey anti-Rat 568	Secondary	1:750	Abcam - ab175475
Flow Cytometry	Rabbit eNOS p602	Primary	1:200	
	Mouse eNOS-647	Primary	20 µL/ 100k cells	BD - 560102
	Donkey anti-rabbit 647	Secondary	1:2000	Abcam - ab150075
Western Blotting	Mouse eNOS	Primary	1:1000	BD - 610297
	Rabbit ERK	Primary	1:1000	CST – CST 9102
	Mouse P-ERK	Primary	1:2000	CST – CST 9106
	Rabbit p38	Primary	1:1000	CST – CST 9212
	Mouse P-p38	Primary	1:2000	CST – CST 9216
	Rabbit P-JNK	Primary	1:1000	CST – CST 9251
	Goat GAPDH	Primary	1:1000	Abcam – ab9483
	Rabbit eNOS P-s1177	Primary	1:1000	R&D systems - MAB9028
	Rabbit eNOS P-s615	Primary	1:500	Abcam - ab138458
	Rabbit eNOS P-t495	Primary	1:1000	CST – CST 9574
	Mouse eNOS P-s632	Primary	1:1000	Abcam – ab76199
	Rabbit eNOS P-s114	Primary	1:1000	Millipore – 07-357